AN INVESTIGATION INTO THE ACCELERATION RESPONSE OF A DAMAGED BEAM-TYPE STRUCTURE TO A MOVING FORCE

A. González[a,b] and D. Hester[c,d,*]

Abstract

In recent years there have been a growing number of publications on procedures for damage detection in beams from analysing their dynamic response to the passage of a moving force. Most of this research demonstrates their effectiveness by showing that a singularity that did not appear in the healthy structure is present in the response of the damaged structure. This paper elucidates from first principles how the acceleration response can be assumed to consist of 'static' and 'dynamic' components, and where the beam has experienced a localised loss in stiffness, an additional 'damage' component. The combination of these components establishes how the damage singularity will appear in the total response. For a given damage severity, the amplitude of the 'damage' component will depend on how close the damage location is to the sensor, and its frequency content will increase with higher velocities of the moving force. The latter has implications for damage detection because if the frequency content of the 'damage' component includes bridge and/or vehicle frequencies, it becomes more difficult to identify damage. The paper illustrates how a thorough understanding of the relationship between the 'static' and 'damage' components contributes

to establish if damage has occurred and to provide an estimation of its location and severity. The findings are corroborated using accelerations from a planar finite element simulation model where the effects of force velocity and bridge span are examined.

Keywords: beam; crack; dynamic; simply-supported; singularities; vibration.

Full postal address:

[a]School of Civil, Structural & Environmental Engineering, University College Dublin, Belfield, Dublin 4, Ireland

[c] SPACE, David Keir Building, Queen's University Belfast, BT9 5AG, UK

Email/Phone/Fax:

[b]arturo.gonzalez@ucd.ie, (P) +353-1-7163219, (F) +353-1-7163297

[d]d.hester@qub.ac.uk, (P) +44-28-90974600,

[*]corresponding author

1. Introduction

The past decade has seen a growing amount of research in the area of Structural Health Monitoring. Farrar and Worden [1] point out that this research is motivated by its potential life-safety and economic impact. Nondestructive damage identification techniques tend to fall into the category of local or global [2]. Localised methods include techniques such as acoustic emission, ultra sonic testing, magnetic field, radiography and eddy current methods. For these experimental methods to work, the vicinity of the damage needs to be known a priori and the area of the structure to be inspected needs to be assessable, which often may not be the case on civil engineering structures. The potential difficulties associated with localised experimental methods has resulted in the development and continued research in global methods of condition monitoring. These methods detect damage by examining changes in the dynamic behavior of the structure. The fundamental principle behind vibration-based damage identification methods is that damage causes a change in the physical properties of the structure (e.g. stiffness, mass, damping). Once the physical properties have been altered, the vibration characteristics of the structure (e.g. natural frequencies, mode shapes, etc.) will change. Therefore by identifying changes in the vibration characteristics, the presence of damage can be detected.

A number of authors have published reviews on the most common vibration-based condition monitoring techniques [2-5]. Broadly speaking these methods can be categorized as: (i) natural frequency based methods, (ii) mode shape based methods and (iii) curvature based methods. The aforementioned methods are applicable across a broad range of engineering structures and their main features are summarized below.

To implement natural frequency-based condition monitoring, it is generally necessary to develop a numerical model of the structure. The numerical model is used to simulate

damage scenarios at various locations in the structure and the corresponding natural frequencies are calculated. Vibration data is then collected from the structure and the damage location/severity is estimated by matching the observed natural frequencies to those calculated by the numerical model [6-8]. Salawu [8] presents a review of papers dealing with the detection of structural damage using frequency changes. He highlights that the advantage of the approach is that resonant frequencies can be measured relatively easily and are typically quite reliable. However, the disadvantages are that frequency changes caused by damage are generally quite small (< 5%) whereas frequency changes of 5-10% due to environmental conditions are not uncommon. Another disadvantage of frequency-based methods is that damage of similar severity at two different locations may cause the same amount of frequency change.

Mode shape-based methods traditionally use differences in mode shapes between healthy and damaged structures as the basic feature for damage detection [9,10]. Compared to natural frequency-based methods, mode shape-based methods have the significant advantage of containing information that makes them more sensitive to local damages. They are also less affected by environmental effects such as temperature [5]. However, the disadvantage of the method is that many sensors are typically required to measure the mode shapes accurately and base line data from an experimental test on the intact structure (or an accurate structural model of the intact structure) is also necessary, but often unfeasible. To overcome the limitation of needing base line data, the development of response-based methods that only need experimental data from damaged structures has become an increasing focus of research. The principle behind this kind of approach is that the mode shapes from a structure that has experienced a localized loss in stiffness will contain a characteristic damage feature that can be extracted by signal processing techniques. The wavelet transform has obvious advantages

when trying to detect these features from mode shape data due to its ability to analyze a local portion of a larger signal [11-14].

Despite the fact that mode shapes contain local information, one of the problems that persist is that the mode shape is not particularly sensitive to small levels of damage [15]. Therefore mode shape curvatures are often used, because typically changes in the curvatures of mode shapes are highly localised in the region of damage. Pandey et al. [16] demonstrate the effectiveness of comparing the mode shape curvatures of healthy and damaged beams to locate damage. They also highlight the superior performance of this approach when compared to just using the displacement mode shapes directly. Other authors have developed signal processing techniques that use modal curvature without a requirement for base line data from the healthy structure [17,18]. In general, mode shape-based and mode shape curvature-based methods are better at locating the damage than natural frequency-based methods. However, the drawback of many mode shape-based methods is the necessity of having measurements from many locations.

The use of finite element model updating to detect damage has been investigated by a number of authors. For this approach to be effective, the user must have a well correlated model of the structure in its undamaged state and experimental data (e.g. natural frequencies and mode shapes) from the damaged structure. Then the engineer must use his/her judgement to select the parameters that are to be updated in the model, so that the behaviour of the updated model matches the behaviour of the real structure. For example, Sinha et al. [19] test finite element model updating on a cantilever beam and results show how the location of damage can be estimated to a high degree of accuracy (error < 5%) and its severity judged reasonably well (error < 30%). Teughels and De Roeck [20] also use finite element updating to identify structural damage in a Swiss highway bridge. Experimental eigenfrequencies and

mode shapes are taken from the healthy and damaged bridge to tune healthy and damaged models. Their updated model successfully identifies the location and severity of damage. Although finite element model updating techniques have been shown to provide high levels of accuracy, they rely on accurate and sufficient experimental data for model calibration which sometimes can prove to be difficult or expensive to undertake.

In recent years, many authors have placed emphasis upon identifying localised damage in a beam from its response to a moving force, e.g., through the application of wavelets to the beam displacement [21,22] or acceleration response [23]. Others have applied empirical mode decomposition to the acceleration response [24,25]. All these approaches have something in common, the damage is visualised through the appearance of a singularity in a processed signal supposed to be smooth in a healthy case. This paper provides a deep insight into the different components that are present in the acceleration response of a beam-type structure when traversed by a moving force and shows how this information can be exploited to improve the sensitivity of a damage detection algorithm based on the response to traffic data. Unlike other frequency-, mode shape- or curvature-based methods, the approach proposed here is model-free, it does not require baseline data from a healthy structure, it is not affected by temperature changes and it only needs a limited number of sensors.

2. Understanding the components of the acceleration response

2.1. *Mathematical model for simulations*

A bridge is modelled as a discretized simply supported finite element beam. The response of the beam to a moving force is solved using the second order matrix differential equation given in Equation (1).

$$\mathbf{M}\,\mathbf{a(t)} + \mathbf{C}\,\mathbf{v(t)} + \mathbf{K}\,\mathbf{y(t)} = \mathbf{f(t)} \tag{1}$$

where **y(t)** contains the vertical displacement and rotation of the degrees-of-freedom of the model, and **v(t)** and **a(t)** their velocities and accelerations respectively. In this model, **M**, **C** and **K** are the consistent global mass, global damping and global stiffness matrices of the bridge which are assumed to be unaffected by the moving force. **f(t)** is the vector of applied forces at each degree-of-freedom, which is calculated by distributing the moving force to the nodes of the underlying element using the hermitian functions [26]. The global stiffness **K** and mass **M** matrices of the bridge are assembled from the elementary stiffness $\mathbf{K_e}$ and mass $\mathbf{M_e}$ matrices given in Equations (2) and (3) respectively for standard 1D beam elements of density ρ, cross-sectional area A, Young's modulus E, length L_e and inertia I [27].

$$\mathbf{K_e} = \begin{bmatrix} \frac{12EI}{L_e^3} & \frac{6EI}{L_e^2} & \frac{-12EI}{L_e^3} & \frac{6EI}{L_e^2} \\ \frac{6EI}{L_e^2} & \frac{4EI}{L_e} & \frac{-6EI}{L_e^2} & \frac{2EI}{L_e} \\ \frac{-12EI}{L_e^3} & \frac{-6EI}{L_e^2} & \frac{12EI}{L_e^3} & \frac{-6EI}{L_e^2} \\ \frac{6EI}{L_e^2} & \frac{2EI}{L_e} & \frac{-6EI}{L_e^2} & \frac{4EI}{L_e} \end{bmatrix} \tag{2}$$

$$\mathbf{M_e} = \frac{\rho A L_e}{420}\begin{bmatrix} 156 & 22L_e & 54 & -13L_e \\ 22L_e & 4L_e^2 & 13L_e & -3L_e^2 \\ 54 & 13L_e & 156 & -22L_e \\ -13L_e & -3L_e^2 & -22L_e & 4L_e^2 \end{bmatrix} \tag{3}$$

Damping is typically low in bridges and its effect on the forced response is neglected here. When the matrices **M** and **K**, and the forcing vector **f(t)** have been populated, Equation (1) can be solved using a discrete time integration scheme [28,29] yielding the unknowns **y(t)**, **v(t)** and **a(t)**. Damage is introduced in the model by allowing for a localised loss in stiffness

due to a crack. Dimarogonas [30] gives an extensive review of the different modelling techniques that can be used to model the damage due to a crack. The stiffness reduction used in this paper is the one proposed by Sinha et al. [19] which quantifies a gradual loss of bending stiffness that extends 1.5 times the depth of the beam at both sides of the crack (Fig. 1). The latter is modelled by introducing a reduced moment of inertia in the elementary matrixes $\mathbf{K_e}$ of those elements close to the crack. Previous work on damaged beams has focused on rectangular beams, where the ratio of crack height (h) to beam depth (d) (denoted as delta in this paper) has often been used to characterize the severity of the damage. Delta values of 0.1 and 0.2 represent 73% and 51% respectively of the inertia of a healthy rectangular section. The same equivalency between delta and associated percentage of the healthy inertia value is maintained for the beam sections used in this paper. Using delta as a measure of damage severity maintains consistency with previous published work and allows meaningful comparison of results. The responses of the damaged beam to a moving force are found to be in agreement with those published by Mahmoud [31]. The numerical integration technique used in the simulations is the Wilson-theta method, further details on the structural model can be found in [23,32,33].

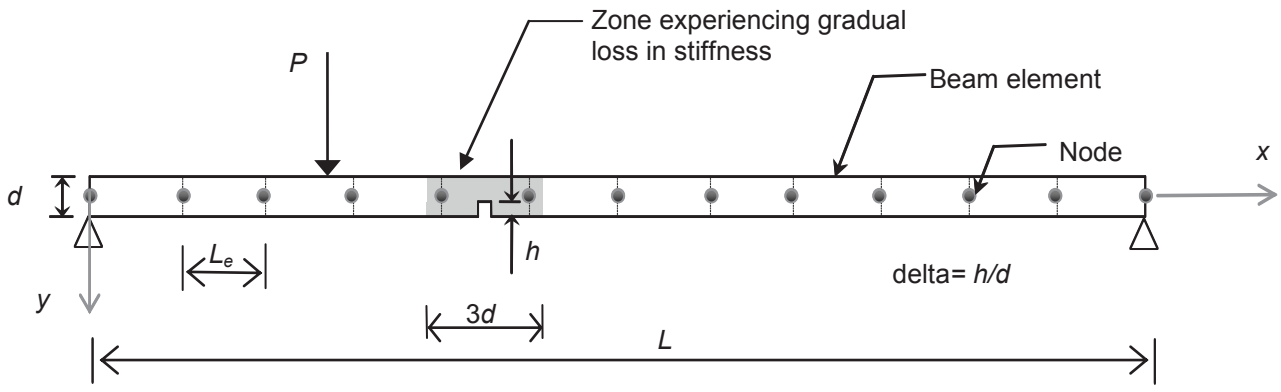

Fig. 1. Sketch of discretised beam model subject to a moving force.

2.2. *Components of different types of response*

To understand why there is a local singularity in the structural response as the force crosses a weakened section away from the measurement point, it is useful to break the total displacement from a damaged beam into a number of components, namely a healthy 'static' displacement $\mathbf{y_{healthy\_static}(t)}$ (i.e., static response of the structure without localised losses of stiffness), a 'damage' static displacement $\mathbf{y_{damage}(t)}$ (i.e., the difference between the static response of the damaged and healthy structures), and a 'dynamic' displacement (i.e., the difference between the total ($\mathbf{y(t)}$ in Equation (1)) and static responses of the damaged beam due to a moving force). The values $\mathbf{y_{healthy\_static}(t)}$ and $\mathbf{y_{damage}(t)}$ can be understood mathematically as follows: $\mathbf{y_{healthy\_static}(t) = K_{healthy}^{-1} f(t)}$ where $\mathbf{K_{healthy}}$ is the matrix stiffness of the structure in a healthy state, and $\mathbf{y_{damage}(t) = y_{static}(t) - y_{healthy\_static}(t)}$ where $\mathbf{y_{static}(t) = K^{-1} f(t)}$. In the latter, $\mathbf{K}$ is the stiffness matrix of the damaged structure as defined in Section 2.1.

Unless otherwise specified, the bridge under investigation has 40 m span length, 15 m width and the cross-sectional properties are based on 10 SY6 precast concrete beams spaced at 1.5 m centres with a 195 mm thick deck slab. The latter results into an inertia of 6.02 m^4 and a cross-sectional area of 10 m^2. A Young's modulus of 3.5×10^{10} N m^{-2} is assumed which leads to a first natural frequency of 2.88 Hz for the healthy structure. The bridge is modelled using 40 discretized beam elements and the time step Δt used in the simulations is 0.0005 seconds. Fig. 2(a) shows the total mid-span displacement as a constant force of 10 tonnes crosses the bridge at 6 ms^{-1}. The bridge has a crack at the 1/3 point of the span with delta equal to 0.2. The *x*-axis in the figure shows the normalised position of the force on the bridge (0 and 1 when the force is at the start and end of the bridge respectively). Figs. 2(b) and 2(c) show the velocity and acceleration of the mid-span section, which are obtained by

differentiating the mid-span displacement once and twice respectively with respect to time. Fig. 2(d) shows the components of the total mid-span displacement. The ‘static’ component refers to the displacement that would be experienced at mid-span if the force was statically applied and moved incrementally across the healthy structure. The ‘damage’ component is the additional static displacement experienced at mid-span due to the presence of damage. It must be noted that the ‘damage’ component is quite small compared to the ‘static’ component and that the maximum value of the ‘damage’ component occurs when the force is at $0.33L$, i.e., over the damaged section. The ‘dynamic’ component is simply the displacement due to the inertial forces of the bridge. If the ‘static’, ‘damage’ and ‘dynamic’ components of displacement are added together, the result is the total mid-span displacement shown in Fig. 2(a). Fig. 2(e) shows the three components of the velocity response, which are obtained by differentiating each of the three components of displacement with respect to time. Similarly, the three components of the acceleration signal (Fig. 2(f)) are established by differentiating the components of the velocity signal. The sum of the three components in Figs. 2(e) and (f) is equal to the total response shown in Figs. 2(b) and (c) respectively. When comparing displacements, velocities and accelerations of the mid-span section, it can be seen that the ‘dynamic’ component becomes increasingly larger with respect to ‘static’ and ‘damage’ components as the order of differentiation of the type of response increases.

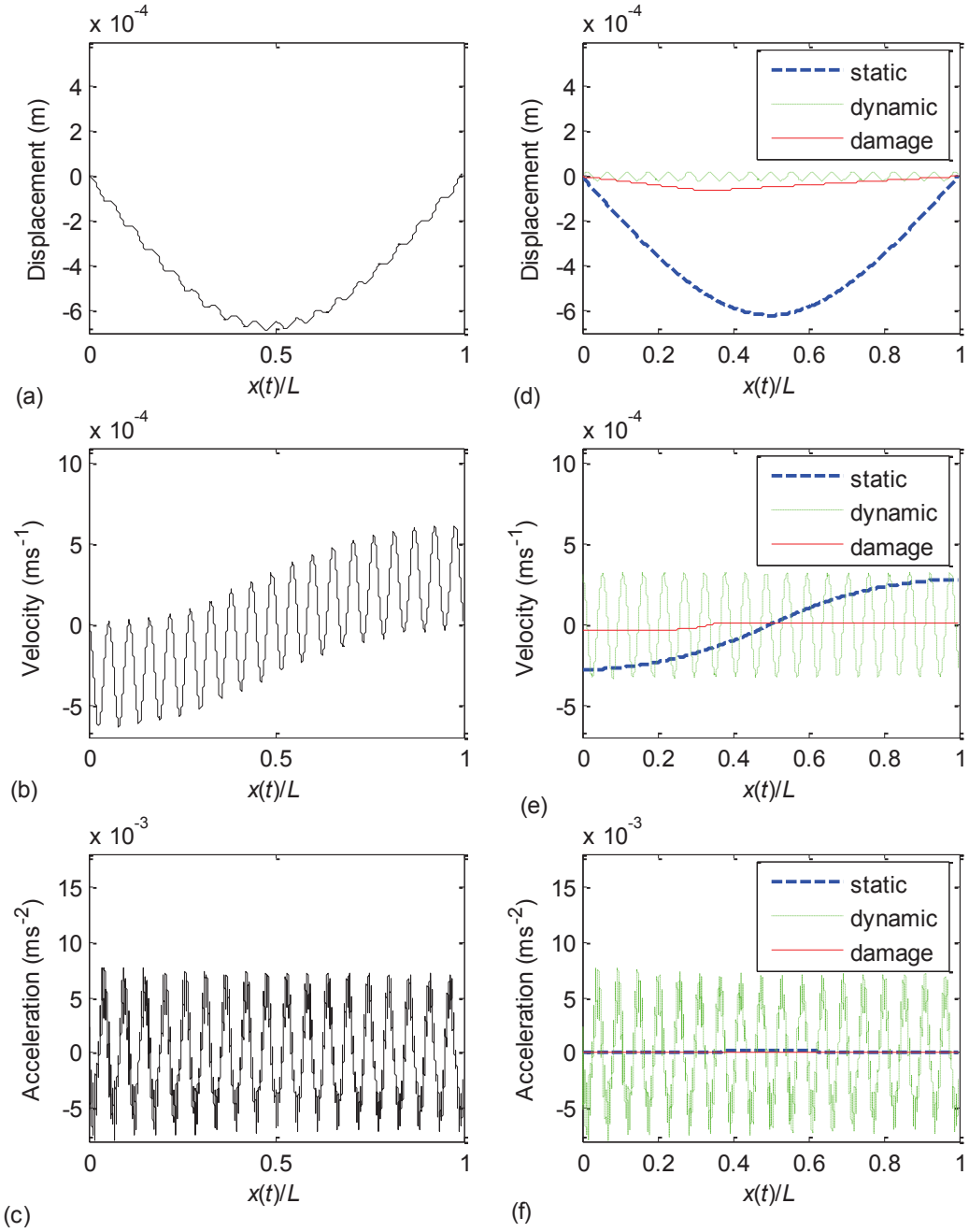

Fig. 2. Total response of the mid-span section and its components due to a force travelling at 6 m s^{-1}: (a) total displacement; (b) total velocity; (c) total acceleration; (d) components of displacement; (e) components of velocity; (f) components of acceleration.

Fig. 2 has shown how damage manifests in three types of responses. However, it may not be easy to record displacements or velocities to the required level of resolution and scanning frequency on site. Therefore, from this point forward this paper focuses on the acceleration response.

2.3. *Effect of velocity on the shape of the singularity*

The 'static' and the 'damage' components of acceleration are very small relative to the 'dynamic' component, thus, they practically look like straight lines in Fig. 2(f). Figs. 3(a), (b) and (c) show the 'dynamic' component of mid-span acceleration due to force velocities of 6, 12 and 24 m s^{-1} respectively, for a 40 m bridge with a delta of 0.2 at the 1/3 point of the span. The 'static' and 'damage' components shown in Figs. 3(d)-(f) are very small relative to the 'dynamic' component and are plotted at a much smaller scale. Figs. 3(a)-(f) show that as the velocity increases, the length of the signals becomes shorter and the amplitude of 'dynamic', 'static' and 'damage' components increase.

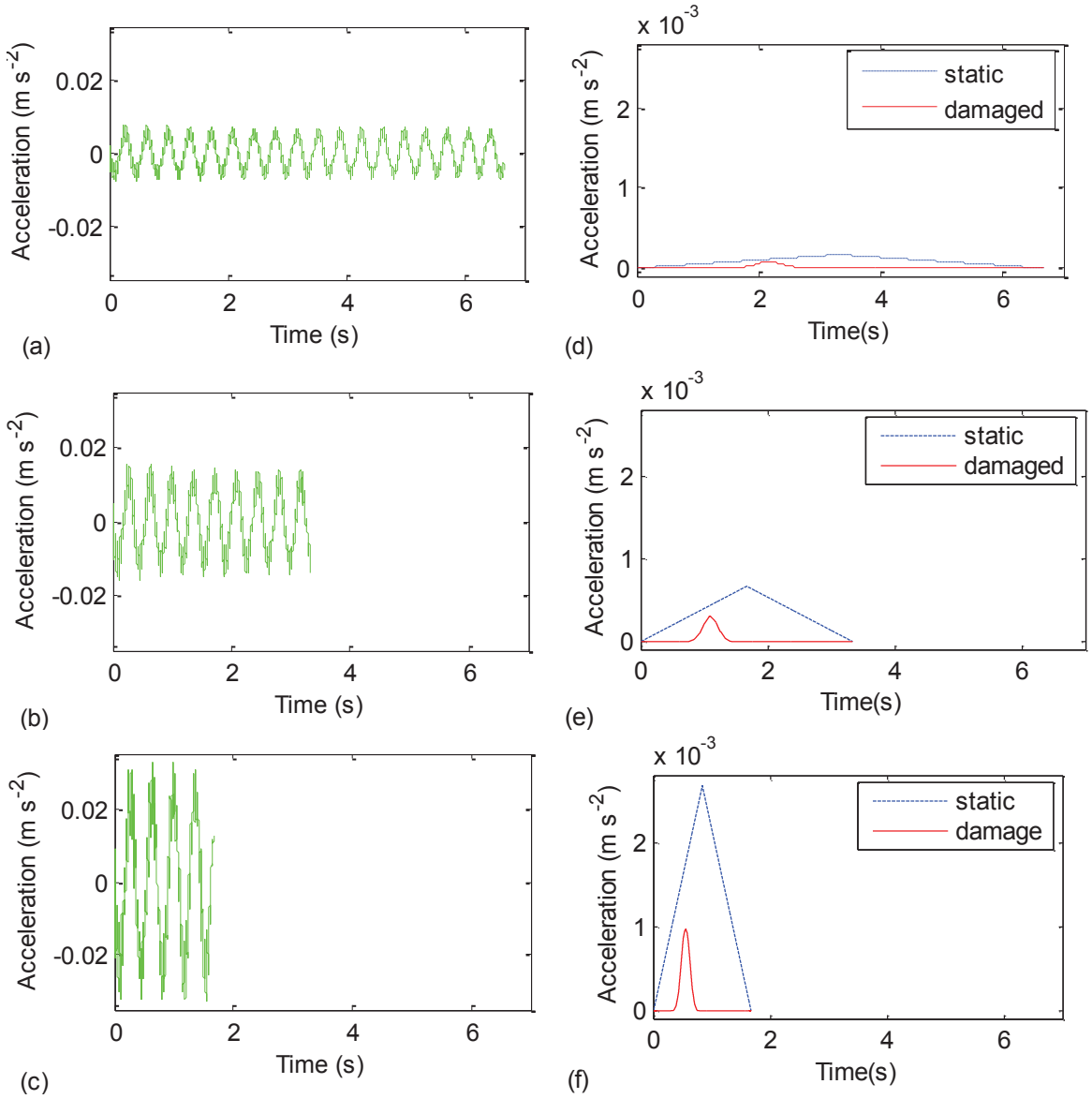

Fig. 3. Time domain representation of the components of mid-span acceleration for different velocities of the moving force: (a) 'dynamic' at 6 m s^{-1}; (b) 'dynamic' at 12 m s^{-1}; (c) 'dynamic' at 24 m s^{-1}; (d) 'static' and 'damage' at 6 m s^{-1}; (e) 'static' and 'damage' at 12 m s^{-1}; (f) 'static' and 'damage' at 24 m s^{-1}.

It can be seen that the 'static' component increases linearly from zero to a maximum at the measurement location, and then decreases linearly back to zero, while the 'damage'

component is zero everywhere except near the damaged location. Therefore, if an appropriate method of filtering the 'dynamic' component out was employed, it should be possible to locate damage in a bridge by analysing its acceleration response. However, to successfully extract particular features within a given signal, it is necessary to have an understanding of the frequency content of its components.

2.4. *Frequency content of acceleration components*

Figs. 4(a)-(c) show the result of calculating power spectral density (PSD) functions for the 'dynamic' components given in Figs. 3(a)-(c), and the dominant frequency of vibration of the bridge is evident, i.e., 2.76 Hz. Figs. 4(d)-(f) show the frequency content of the 'static' and 'damage' components given in Figs. 3(d)-(f). One significant difference between the PSD of the 'dynamic' component and the PSD of the 'static' and 'damage' components is in relation to the range of frequencies that they cover in the spectrum. The PSD of the 'dynamic' component shows one distinctive narrow peak at the first natural frequency given by the main mode of vibration of the beam, whereas the PSD of the 'static' and 'damage' components occurs across a broader range of frequencies. Fig. 4(d) shows the frequency content of the 'static' and 'damage' components when the velocity of the force is 6 m s^{-1}. The PSD content of the 'static' component primarily occupies the range of frequencies 0.0 Hz - 0.3 Hz while the 'damage' component approximately occupies the range of frequencies 0.0 – 1.45 Hz. Fig. 4(e) shows the frequency content of the 'static' and 'damage' components when the velocity of the force is 12 m s^{-1}. This time, most of the PSD content of the 'static' component is contained between 0.0 Hz and 0.6 Hz. By increasing the velocity of

the force from 6 m s^{-1} to 12 m s^{-1}, the 'static' component has shortened by a factor of 2 in the time domain (Figs. 3(d) and (e)), so naturally the upper frequency of the 'static' component has also increased by a factor of 2. Similarly, the upper limit of the frequency range defining the 'damage' component has increased from 1.45 Hz to 2.9 Hz when the velocity is doubled. Fig. 4(f) shows the frequency content of the 'static' and 'damage' components when the velocity of the force is 24 m s^{-1}. For this velocity, the PSD content of the 'static' component mostly occupies the range of frequencies 0.0 Hz - 1.2 Hz and the upper frequency limit of the 'damage' component is approximately 5.8 Hz. For a velocity of 6 m s^{-1}, the first natural frequency of the bridge (2.76 Hz) falls out of the zone of influence of the 'damage' component (0.0-1.45 Hz). However, for a velocity of 12 m s^{-1}, and more clearly 24 m s^{-1}, the first natural frequency of the bridge associated to the 'dynamic' component falls within the zone of frequencies occupied by the 'damage' component which will make it difficult to separate both components. The latter explains the falloff in the performance of damage detection techniques with increasing velocity of the moving force reported in the literature [33].

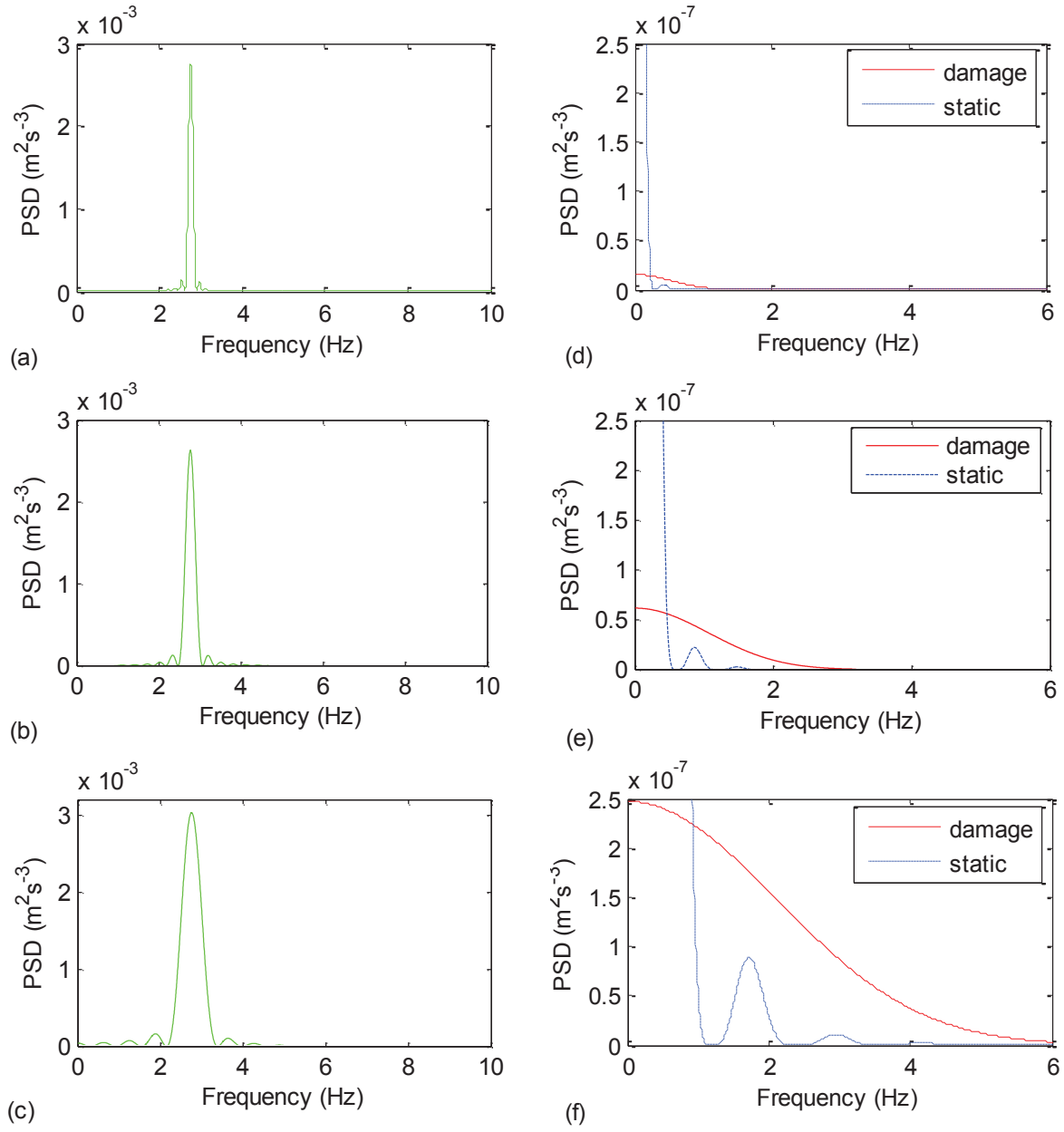

Fig. 4. Frequency content of acceleration components for different velocities: (a) 'dynamic' component at 6 m s^{-1}; (b) 'dynamic' component at 12 m s^{-1}; (c) 'dynamic' component at 24 m s^{-1}; (d) 'static' and 'damage' components at 6 m s^{-1}; (e) 'static' and 'damage' components at 12 m s^{-1}; (f) 'static' and 'damage' components at 24 m s^{-1}.

3. Locating damage

In Section 2, the total response has been divided in a number of components to visualize the damage-related frequency content to be targeted by a damage detection algorithm. Essentially, the goal is to use a signal processing technique to expose the 'damage' component of the acceleration signal if present. A Moving Average Filter (MAF) has been found to provide a robust approach to remove the 'dynamic' component and crucially has the advantage of maintaining the area under the 'damage' curve (the significance of this will be dealt with in more detail later). A MAF replaces each point in the signal, a(t), at an instant *t*, with the average $\bar{a}(t)$ of several adjacent points. More precisely the average is calculated here from an equal number of data points either side of a central value as in Equation (4).

$$\bar{a}(t) = \frac{1}{M} \sum_{j=-(M-1)/2}^{(M-1)/2} a(t + j\Delta t) \qquad (4)$$

where Δt is the time step between consecutive inputs and *M* is the span of the MAF. For example if *M* is 7, point 20 of the filtered signal is found by calculating the average of points 17 to 23 of the input signal *a(t)*. If the acceleration signal in Fig 2(c) is examined, it can be seen that a given period of vibration has an approximately equal measure of positive and negative parts. Therefore if the span of the MAF is set to equal one period of vibration, the positive and negative parts will cancel each other out and as a result most of the dynamic oscillations will be removed. The dominant frequency of vibration of the total mid-span acceleration response shown in Fig. 2(c) (20 m bridge with a delta of 0.2) is found to be 2.76 Hz (Fig. 4(a)), therefore the period of vibration is 0.362 seconds. The scanning frequency used to generate the acceleration is 2000 Hz, consequently a MAF with an *M* value of (2000*0.362=) 724 points will remove the first natural frequency. Fig. 5(a) shows the result

of applying the MAF to the acceleration of Fig. 2(c). It can be seen that there is a localised bump in the acceleration signal at approximately $x(t)/L = 0.33$, i.e., when the force stands over the damaged location. However, some high frequency components are present and neither the 'static' nor 'damage' components are particularly clear. Simply applying the same MAF a second time removes much of the remaining vibration and much clearer 'static' and 'damage' components are obtained. So, Fig. 5(b) exposes the triangular shape of the 'static' component as well as the localised bump at $0.33L$ which is the location of the damage.

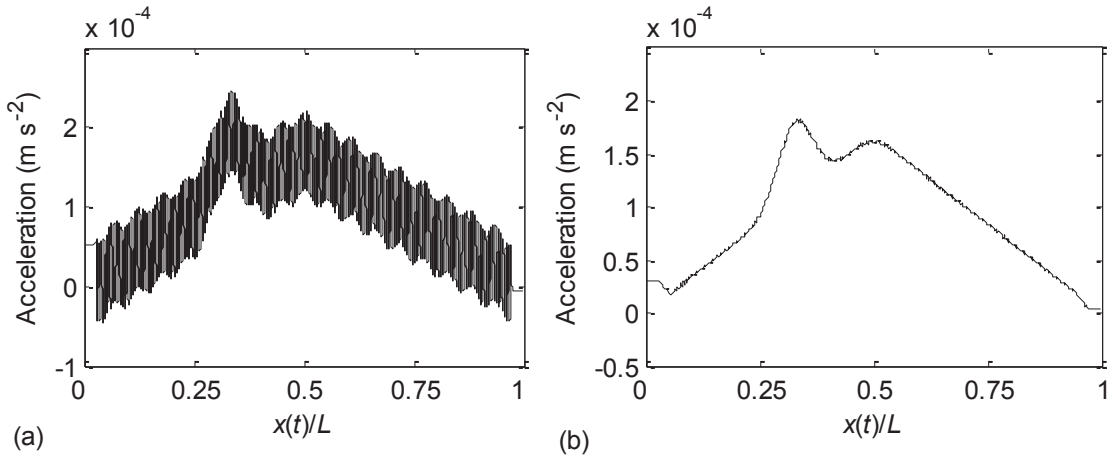

Fig. 5. Filtered total acceleration (a) after applying MAF once; (b) after applying MAF twice.

The effect of the dual application of the MAF to each component of acceleration shown in Fig. 2(f) is examined in Figs. 6(a), (b) and (c). Fig. 6(a) shows the 'dynamic' component of the acceleration signal as well as the result of applying the MAF twice to the 'dynamic' component which reduces it to an horizontal line. Fig. 6(b) shows the theoretical 'static' and 'damage' components, and also the result of applying the MAF twice to the 'static' and 'damage' components. It can be seen that 'static' component is essentially unaffected by the MAF. This is not surprising because the 'static' component has significantly lower frequency content than the frequency that the MAF is trying to remove

(Fig. 4(d)). However, the ‘damage' component covers a broader range of frequencies than the ‘static’ component and it can be altered by the MAF to some extent, i.e., its amplitude and base can be reduced and widened respectively. Finally, Fig. 6(c) shows the PSD of the different components before and after the application of the MAF. The PSD of the ‘dynamic’ component shown in Fig. 4(a) before the application of the MAF, has effectively been reduced to zero in Fig. 6(c) after the application of the MAF. . The ‘static’, ‘filtered static’, ‘damage’ and ‘filtered damage’ plots in Fig. 6(c) are the PSD of the respective components in Fig. 6(b). The PSD of the ‘static’ component remains essentially unchanged by the application of the MAF. Unlike the ‘static’ component, it can be seen that the MAF has reduced the amplitude of the PSD of the ‘damage’ component significantly.

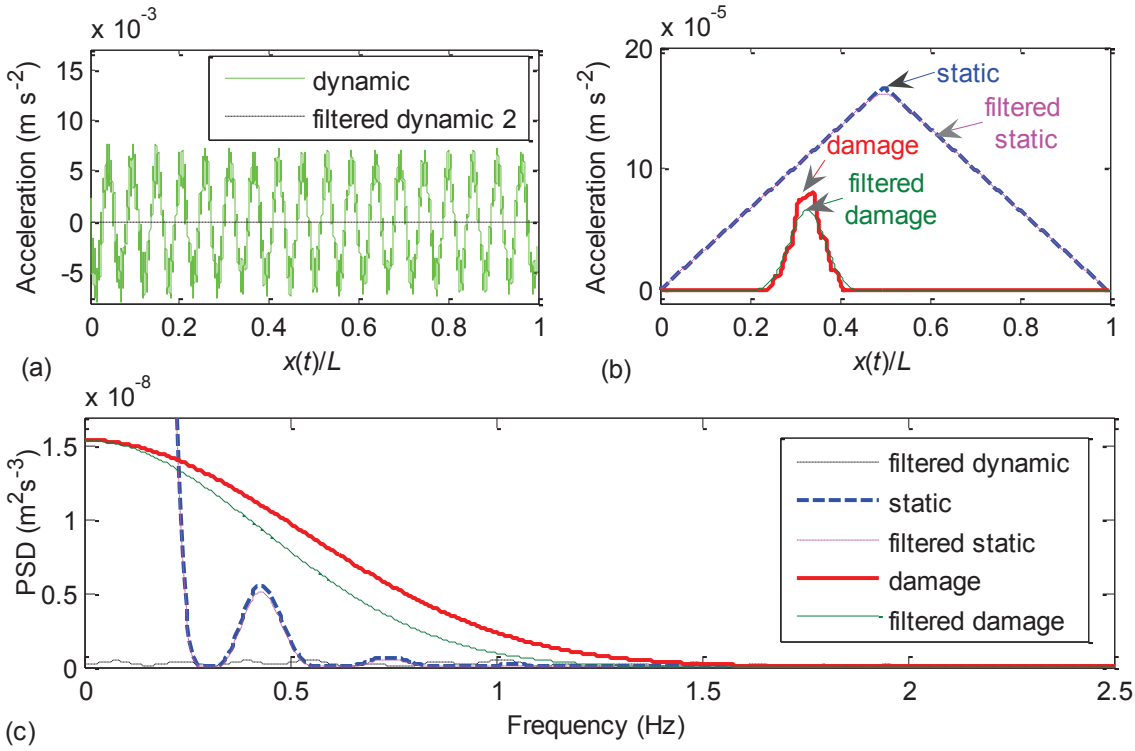

Fig. 6. Filtered (after applying MAF twice) and original (before applying MAF) acceleration components: (a) ‘dynamic’ component in time domain; (b) ‘static’ and ‘damage’ components in time domain; (c) Acceleration components in frequency domain.

It has been seen that applying a MAF to the total acceleration response is effective at removing the 'dynamic' component of the acceleration signal, while hardly affecting the 'static' component but possibly altering the original 'damage' component to some extent. The influence of the MAF on the 'damage' component is investigated in Fig. 7 for velocities of 6, 12 and 24 m s^{-1}. It can be seen how the reduction in amplitude and broadening of the base of the 'damage' component is more pronounced at higher velocities.

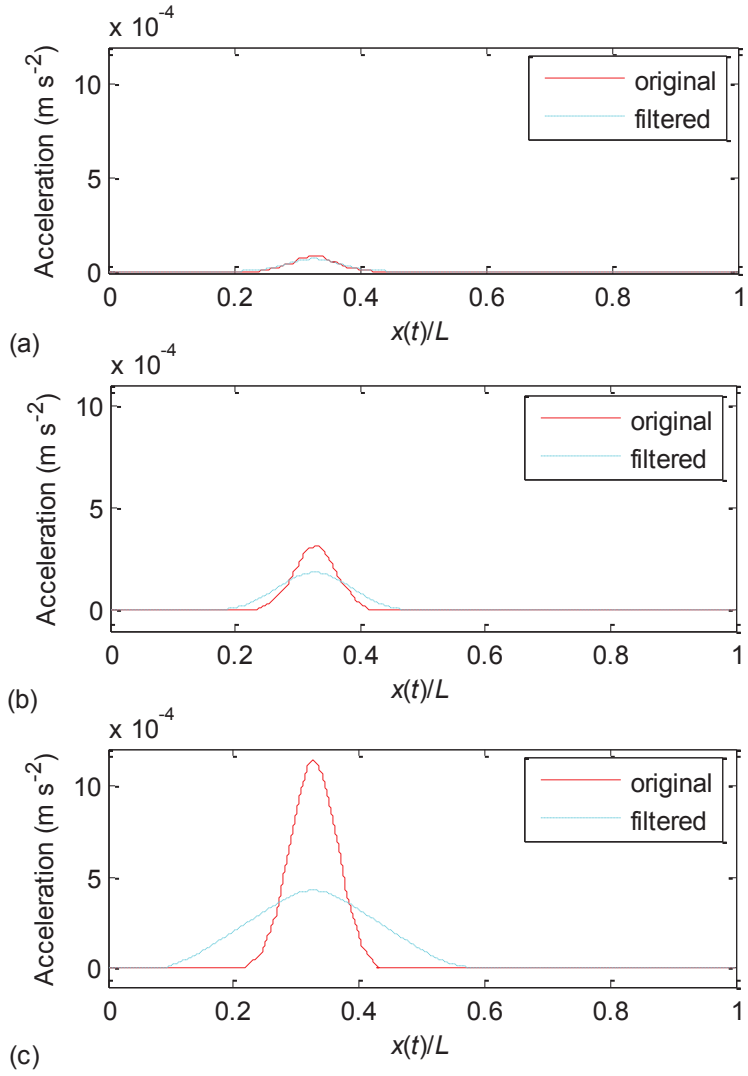

Fig. 7. Effect of MAF on 'damage' component for force velocities of: (a) 6 m s^{-1}; (b) 12 m s^{-1}; (c) 24 m s^{-1}.

When the velocity of the force was 6 m s^{-1} (Fig. 5(b)), it was possible to clearly identify the damage location because the amplitude of the 'damage' component was substantial with respect to the amplitude of the 'static' component. At 24 m s^{-1}, the amplitude of the 'damage' component has been considerably reduced through the filtering process (Fig. 7(c)) and it is more difficult to identify damage (Fig. 8). If the amplitude of the 'damage' component is to be used to quantify damage, the vehicle velocity and smoothing effect of the MAF will need to be taken into consideration. However, the MAF has the property of maintaining the area under the 'damage' component, i.e. the area under each of the dashed (after filtering) curves in Figs. 7(a)-(c) is the same as the area under the solid curves (before filtering). This feature is exploited later in the paper to develop an area based algorithm that can identify damage at higher velocities.

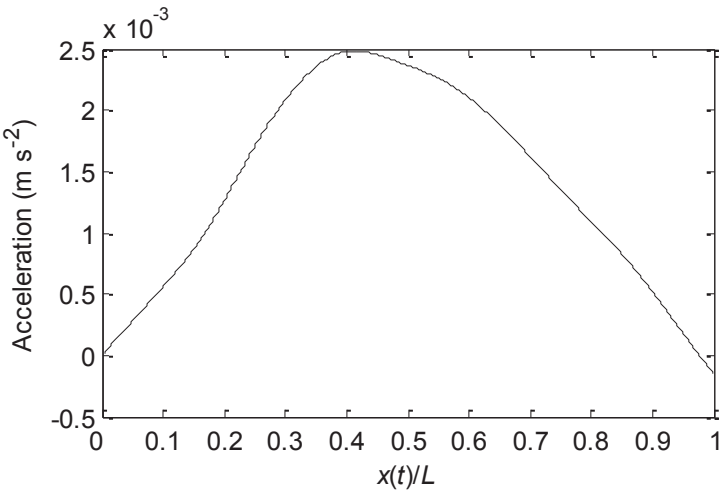

Fig. 8. Total acceleration due to a force travelling at 24 m s^{-1} after applying twice a MAF.

4. Quantifying damage

Section 3 has shown that it is possible to locate a localised loss of stiffness using appropriate filtering. This section intends to provide the operator a way to correctly interpret the severity of the located damage. Therefore if the acceleration signal recorded on a bridge could be separated into 'static' and 'damage' components, it should be possible to quantify the severity of the damage by subsequently comparing both components.

The first step towards facilitating a procedure to quantify damage is to examine how the 'damage' component changes for various damage scenarios. The 'damage' components of the mid-span acceleration of a 40 m span with different damages traversed by a 10 tonne force at 6 m s^{-1} are shown in Fig. 9. The figure illustrates 'damage' components for two damage severities (delta = 0.1 and delta = 0.2) and three different damage locations (0.2L, 0.33L and 0.5L). A plot showing the result of filtering the total acceleration of the healthy bridge is also included in the figure (Essentially the 'dynamic' component is removed from the acceleration signal so all that remains is the 'static' component). The filtering procedure consists of initially applying a low pass filter to remove noise and higher modes of vibration (this is particularly important when dealing with real signals or responses from complex vehicle bridge interaction models with interference of frequencies other than the dominant bridge frequency). It is found that setting the cut-off frequency of the low pass filter to approximately 4 times the dominant mode of vibration ensures that the 'static' and 'damage' components of the response remained unaffected. Then, the dominant mode of vibration is removed using a MAF as described in Section 3. However, before applying the MAF each end of the signal is padded with a copy of opposite sign of itself. The purpose is to reduce the distortion that occurs at the ends of the signal derived from filtering a finite time series. Some

boundary effects are unavoidable, and even padding prior to filtering, a minor distortion still appears at the right hand end of the acceleration.

Obviously the amplitude of the 'damage' component increases as the severity of the damage increases at a given location, but it varies for each location. For a damage of delta = 0.2 at 0.25*L*, 0.33*L* and 0.5*L*, the 'damage' component has maximum amplitudes of 0.47×10^{-4} m s^{-2}, 0.77×10^{-4} m s^{-2} and 1.17×10^{-4} m s^{-2} respectively. Therefore, if damage is to be quantified, it will not simply be a matter of comparing the size of the 'damage' component to the size of the 'static' component, given that the distance from the measurement point to the 'damage' peak must be taken into account.

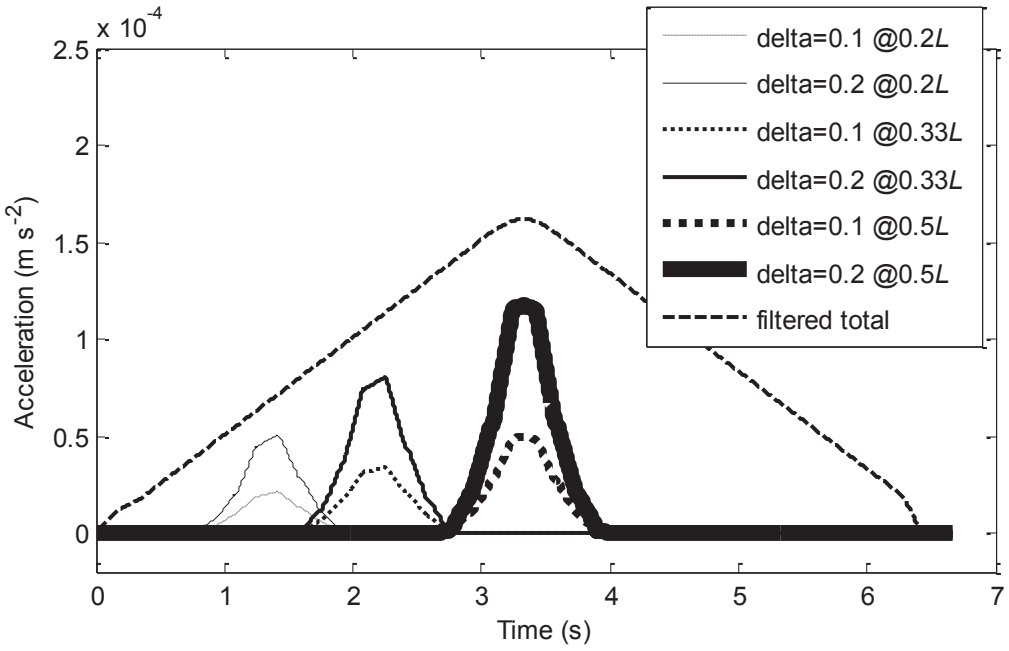

Fig. 9. Estimated 'static' (or filtered total) and 'damage' components for different damage scenarios in a 40 m bridge traversed by a force at 6 m s^{-1}.

The passage of a single point force of 10 tonnes is then simulated at velocities of 6, 12 and 24 m s^{-1} over 10, 20 and 40 m bridge spans. Table 1 provides the properties adopted for the three bridge spans.

Table 1 – Parameters of bridge models.

span (m)	width (m)	inertia (m^4)	modulus of elasticity (N m^{-2})	area (m^2)	1st natural frequency (Hz)
40	15	6.00	$3.5x10^{10}$	10.0	2.88
20	15	1.36	$3.5x10^{10}$	7.3	6.24
10	15	0.28	$3.5x10^{10}$	9.1	10.40

Damage severities of delta = 0.1 and delta = 0.2 are introduced at 0.2*L*, 0.33*L* and 0.5*L* of each span under investigation. For a given damage location and severity, the ratio of the area under the 'damage' curve to the area under the 'static' curve is found to be approximately equal regardless the force velocity and bridge span. Moreover if the ratios obtained for the three spans are all plotted together with respect to the position of the damage, those with the same damage severity (i.e., delta = 0.1 data or delta = 0.2 data) are practically linear as shown by the trend line in Fig. 10. The means of the ratios obtained for all spans/velocities are also plotted in the figure and they sit almost exactly on the trend line, i.e., for a given delta, the ratio is proportional to the distance between the damaged location and the mid-span measurement point. The significance of Fig. 10 is that the information portrayed in it can be used to construct damage contours, i.e., a line that defines a given level of damage (delta = 0.1 contour, delta = 0.2 contour, etc.). Therefore, it will be possible to

estimate the damage severity by merely calculating the ratio of ‘damage’ to ‘static’ areas and locating this point on a damaged contour drawing.

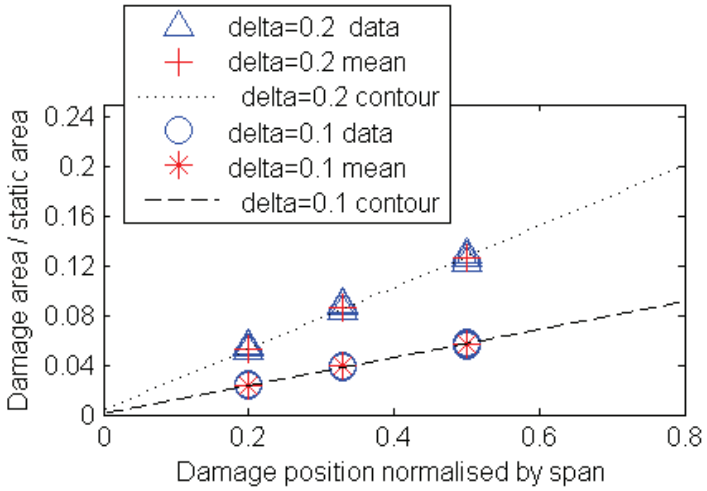

Fig. 10. Ratios of ‘damage’ area to ‘static’ area with respect to the position of damage.

When the simulated acceleration of Fig. 2(c) is filtered using a MAF, the ‘dynamic’ component is removed and Fig. 5(b) made of ‘static’ and ‘damage’ components results. In order to calculate ‘damage’ and ‘static’ area ratios to assess the damage severity, first it is necessary to separate these two components. For this purpose, from Section 2, it is understood that the ‘static’ component of the acceleration response is triangular in nature, i.e., zero when the force is over the supports and maximum when the force is at the measurement point. The ‘static’ component of acceleration at mid-span, $a_s(t)$, due to a single force of magnitude P travelling at velocity v is symmetric and it is given by Equation (5) when the force is located between the left hand support and mid-span.

$$a_s(t) = \frac{Pv^3 t}{2EI} \tag{5}$$

where t is time, and E and I are Young's modulus and inertia respectively. Using an iterative process, a series of triangles of different heights is postulated and subject to the same MAF as the original acceleration prior to comparisons. Then, that filtered triangle that gives a better correlation with the filtered total acceleration is used to establish the 'static' component. The 'static' triangle/component shown in Fig. 11 is obtained using this procedure. Finally, the 'damage' component can be extracted by subtracting the estimated 'static' component from the filtered total acceleration.

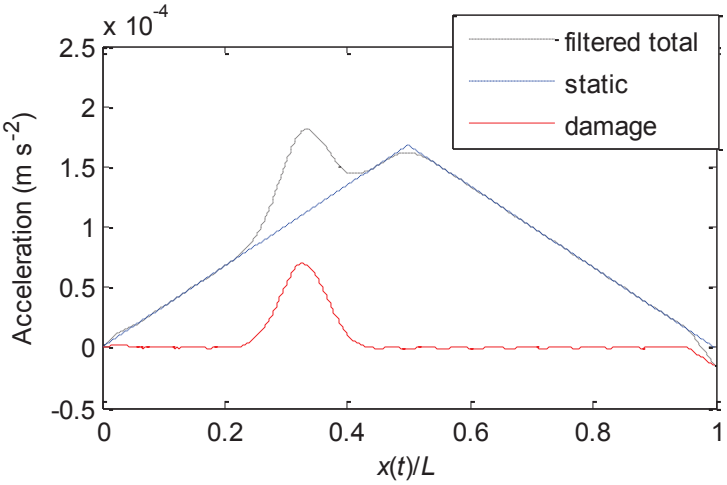

Fig. 11. Extraction of 'damage' component from filtered total acceleration.

The 'static' area is determined by calculating the area under the 'static' triangle and the 'damage' area is found by calculating the area under the 'damage' plot. For the case in Fig. 11, the ratio of 'damage' area to 'static' area is found to be 0.078. This ratio (labelled '40m, 0.2@0.33L,6m/s') is simply plotted on the general damaged contour drawing of Fig. 12 to quantify the severity of the damage. The delta = 0.1 and delta = 0.2 contours in Fig. 12

are reproductions of the lines in Fig. 10. The *x*-coordinate of this data point locates the damage, and it corresponds to the *x*-coordinate of the point of maximum value in the associated 'damage' plot of Fig. 11. Fig. 12 shows that by just calculating the ratio of 'damage' to 'static' areas of the filtered mid-span acceleration, it is possible to correctly identify the location and severity of the damage based on pre-established delta contours. The effectiveness of the proposed damage identification procedure is also illustrated in Fig. 12 for other bridge spans with different damages under a constant force moving at a range of velocities.

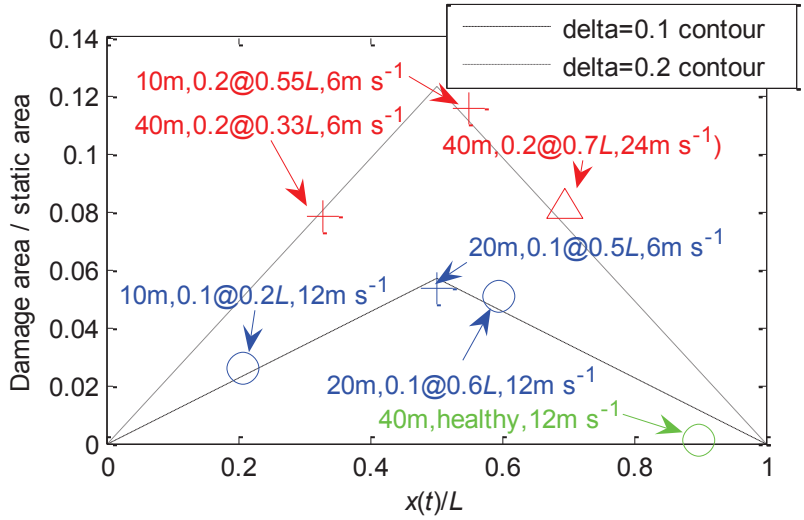

Fig. 12. Location and quantification of damage based on the prediction of ratio 'damage' to 'static' area obtained for different damage scenarios ('40m,0.2@0.33*L*, 6 m s^{-1}' in the figure indicates the bridge had a 40 m span with a damage of delta = 0.2 at 0.33*L* and was traversed by a force at 6 m s^{-1}).

By dividing the 'damage' curve into a number of zones and calculating the area under each zone, multiple damage locations can also be identified and quantified. For example, Fig. 13(a) shows the result of analysing the mid-span acceleration from a 40 m bridge with two damage zones, damage 1 (crack of delta = 0.1 at 0.3*L*) and damage 2 (crack of delta = 0.2 at

0.66L) when traversed by a 10 tonne force travelling at 6 m s^{-1}. The ratio of 'damage' area to 'static' area for damages 1 and 2 are indicated on Fig. 13(b) using triangular and circular data markers respectively. Fig. 13(b) also shows the performance of the algorithm when the the same damage is modelled but the bridge has a modal damping ratio of 3%. The latter is implemented assuming Raleigh damping in accordance with [35]. It can be seen that the consideration of bridge damping makes little difference to the results obtained. This is not surprising given the light damping (typically found in bridges), which will only reduce the amplitude of the total forced response to a small extent, and it will have a relatively small influence on the accurate extraction of 'static' and 'damage' components.

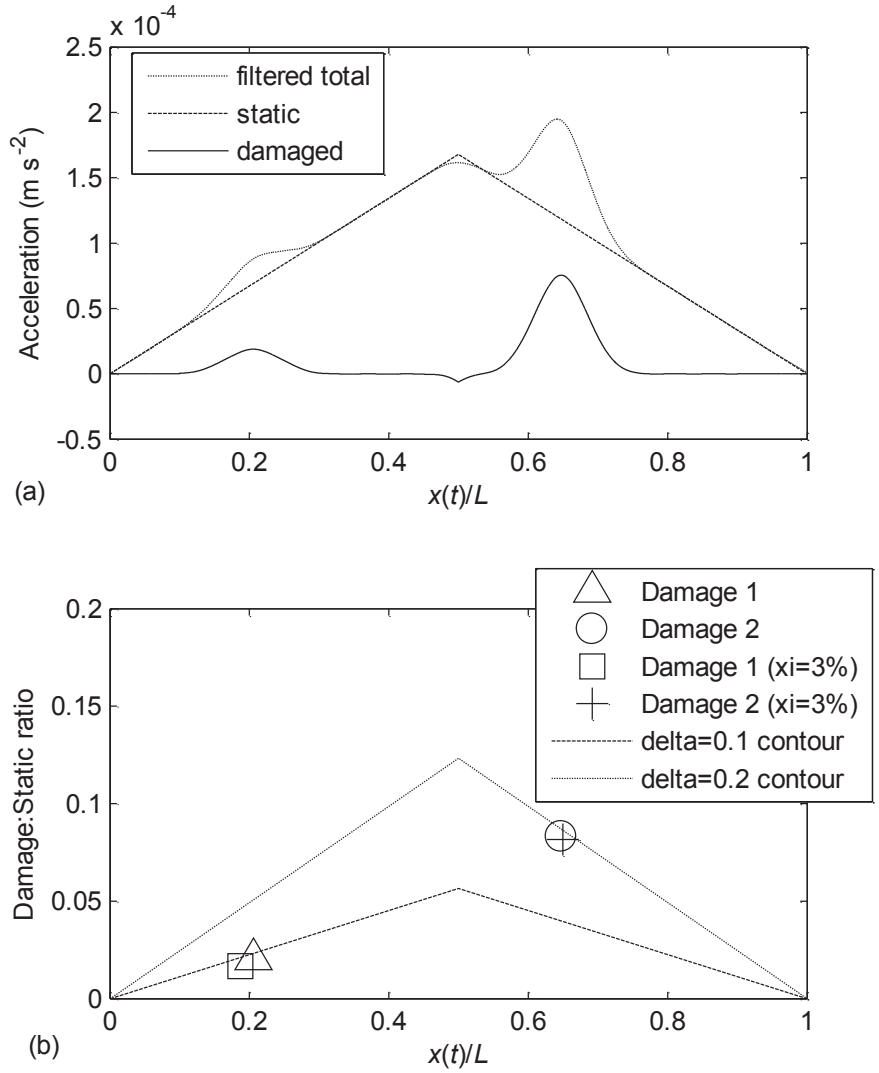

Fig. 13. Detecting multiple damages (a) Extraction of 'damage' component from filtered mid-span acceleration with two damaged locations; (b) location and quantification of damage based on ratio of 'damage' to 'static' area for two different levels of damping.

5. Identification of damage when the bridge is traversed by a two-axle vehicle model

5.1. *Use of the beam acceleration due to two moving constant forces*

Fig. 14(a) shows the total mid-span acceleration due to two constant forces crossing a 40 m bridge with a delta = 0.2 crack at the 1/3 point of the span at 6 m s^{-1}. The magnitudes of the first and second forces are 5 and 10 tonnes respectively and the distance between forces is 5.5 m. The first thing to note in Fig. 14(a) is that there is an abrupt change in the amplitude of the total acceleration signal when the rear axle enters the bridge (0.91 s) and when the front axle leaves the bridge (6.66 s). Fig. 14(b) shows the 'dynamic' component of the acceleration response and the same abrupt changes in amplitude are evident as the axles pass on and off the bridge. Fig. 14(c) shows the 'static' and 'damage' components of the acceleration response. The slope of the 'static' component changes abruptly as the axles cross the measurement location and again as they pass on and off the bridge. The 'damage' component shows two peaks, i.e., one per axle crossing over the damaged location.

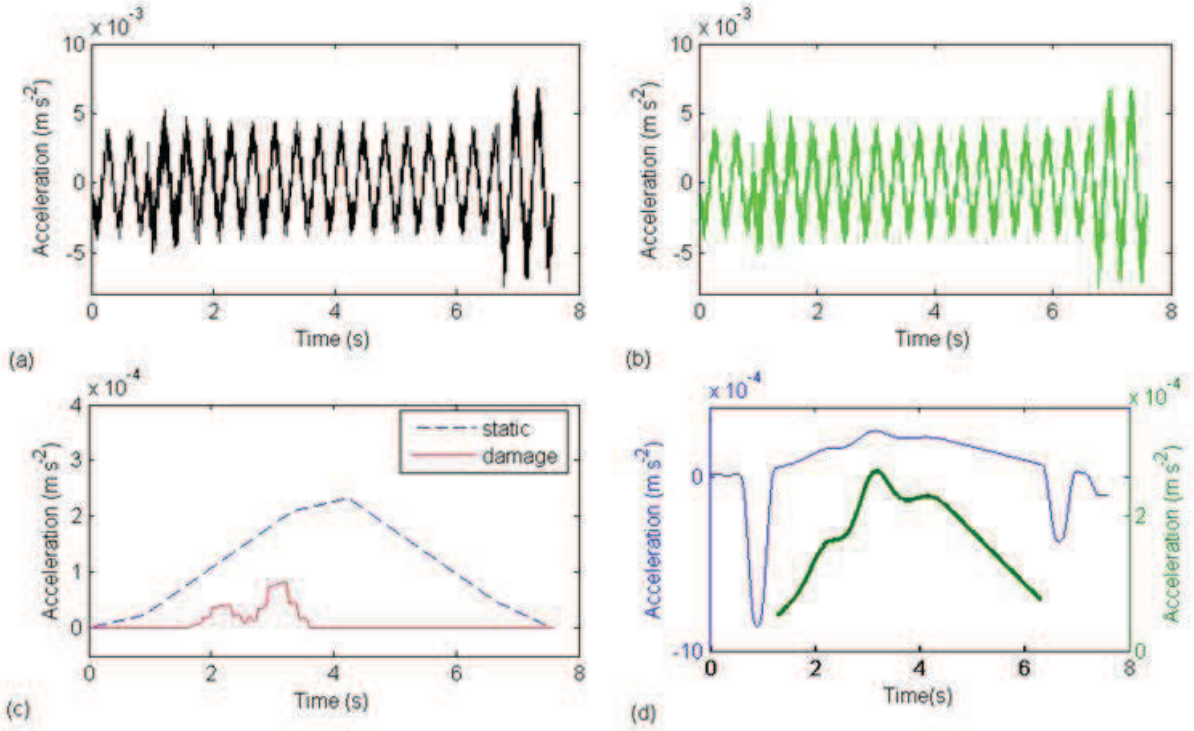

Fig. 14. Mid-span acceleration response due to two constant forces crossing a 40 m bridge: (a) total acceleration response; (b) ' dynamic' component of acceleration; (c) 'static' and 'damage' components of acceleration; (d) filtered total acceleration.

The ordinates of the solid plot in Fig. 14(d) correspond to the main vertical axis and it shows the result applying the MAF to the signal in Fig. 14(a). The filtered signal is dominated by two large troughs at 0.91 and 6.66 seconds as the axles enter and leave the bridge. The heavy plot in Fig. 14(d) corresponds to the secondary vertical axis and it is a magnified view of the central portion of the filtered signal (in effect the sum of the components shown in Fig. 14(c)). Unlike the case of a single constant force, here the 'static' component is no longer triangular, and there are two damage peaks in the 'damage' component even though there is only one damaged location. However by recognising that the 'static' and 'damage' components shown in Fig. 14(c) are simply the sum of the individual axles shifted in time and by assuming the principle of superposition applies to 'static' and 'damage' components, it is possible to recreate the 'static' and 'damage' components due to a single moving point force. González [36] and OBrien et al. [37] describe alternative approaches to calculate the bridge response due to a single moving point force from the bridge's response to the passage of a multi-axle vehicle of known axle weights and spacings (i.e., by shifting and scaling the signal). Once the response of the truck is obtained as if it was applied as a single point force, the same damage detection technique developed in Section 4 for one moving force can be implemented for multi-axle vehicles.

Using this technique, Fig.15 shows the estimated area ratios for three bridge spans (10, 20 and 40 m), two velocities (6 and 24 m s^{-1}) and two damage severities: delta = 0.1 and delta = 0.2 at the 1/3 point. For the 20 m and 40 m spans the damage is correctly identified for both velocities and damage severities. For the 10 m span and a velocity of 6 m s^{-1}, the damage of delta = 0.2 is identified correctly, and the damage of delta = 0.1 is estimated with a reasonable degree of accuracy. However, when the velocity of the force is 24 m s^{-1}, damage

cannot be identified in the 10 m span. The source of this inaccuracy is the relative large wheelbase of the vehicle (5.5 m) compared to the bridge span (10 m), and the short length of the usable signal between the rear axle entering the bridge and the front axle leaving which makes the accurate reconstruction of the 'damage' component very difficult.

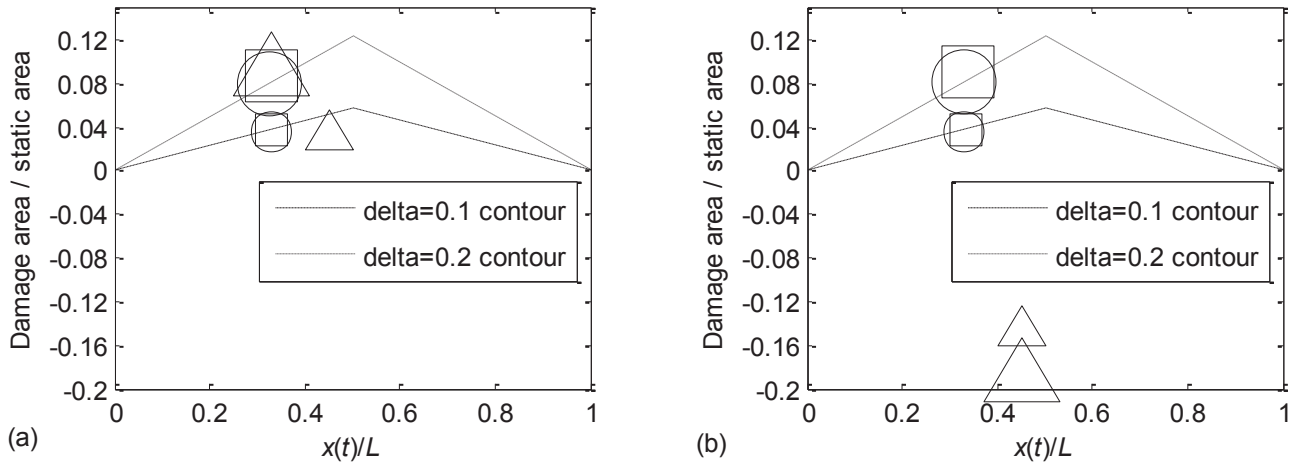

Fig. 15. Location and quantification of damage based on prediction of ratio 'damage' to 'static' area obtained from mid-span accelerations due to two-constant forces for different damage scenarios. Span (m): O 40, □ 20 and Δ 10; damage severity: delta = 0.2 (large marker size) and delta = 0.1 (small marker size). (a) velocity 6 m s^{-1}, (b) velocity 24 m s^{-1}.

5.2. *Use of the beam acceleration due to a 2-axle sprung model on a smooth road profile*

A planar vehicle-bridge interaction simulation model is implemented using the iterative approach described in [23,38,39]. The vehicle represents a 2-axle rigid truck with four degrees of freedom: the pitch and vertical displacement of the sprung mass and the displacement of the two unsprung masses. The properties of suspensions and tyres are similar to those of a semi-tractor unit with twin wheels in the rear axle and are summarized in Table

2, [40,41]. The natural frequencies of the vehicle for bounce, pitch, and front and rear axle hops are 1.43 Hz, 2.07 Hz, 8.60 Hz and 10.22 Hz respectively.

Table 2. Parameters of vehicle model.

dimensional data (m)		
	wheel base	5.5
	dist from centre of mass to front axle	3.63
	dist from centre of mass to rear axle	1.87
	overall length of truck	6.5
mass and inertia		
mass (kg)	front axle mass	700
	rear axle mass	1,100
	sprung body mass	13,300
inertia (kg m^2)	pitch moment of inertia of truck	41,008
suspension		
spring stiffness (kN m^{-1})	front axle	400
	rear axle	1,000
damping (kN s m^{-1})	front axle	10
	rear axle	10
tyre stiffness (kN m^{-1})	front axle	1,750
	rear axle	3,500

Fig. 16 shows the result of analysing a series of mid-span accelerations when the bridge is loaded by the sprung model defined in Table 2. The damage scenarios are the same as those presented in Fig. 15. Again, the simulations of the 10 m bridge lead to inaccurate results (particularly when traversed at 24 m s^{-1}) due to the corruption of large part of the

response by axles entering and leaving the bridge. For the rest of simulations, damage is identified to a reasonable degree of accuracy, although there is a slightly greater spread of the data points than observed in Fig. 15 due to relatively less smooth filtered signals.

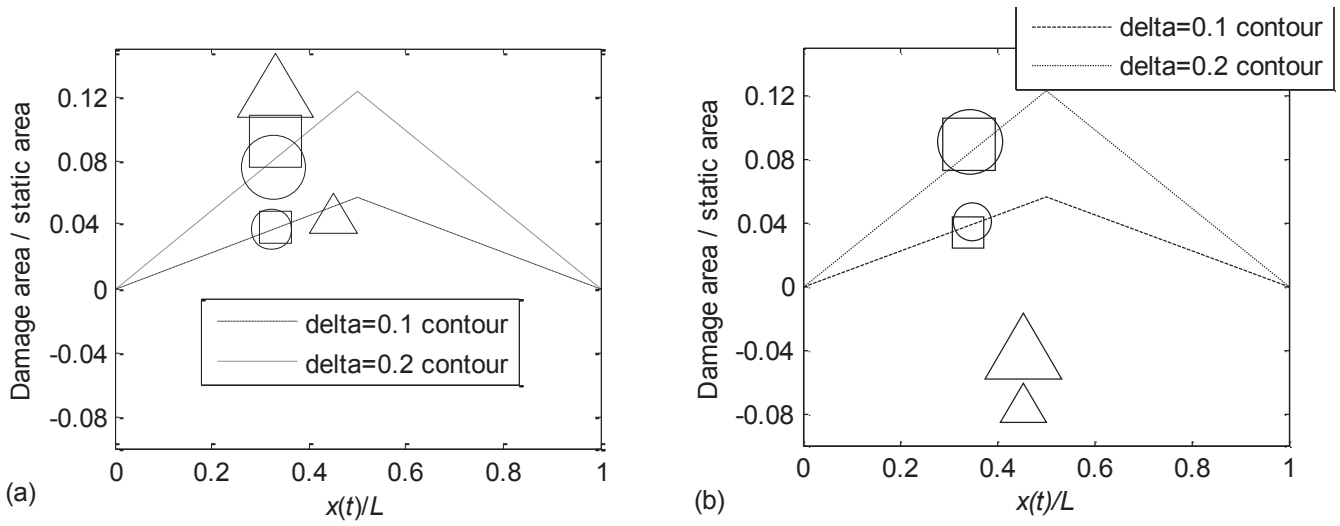

Fig. 16. Location and quantification of damage based on ratio 'damage' to 'static' area obtained from mid-span accelerations due to a two-axle sprung vehicle model on a smooth profile for different damage scenarios. Span (m): O 40, □ 20 and Δ 10; damage severity: delta = 0.2 (large marker size) and delta = 0.1 (small marker size). (a) velocity 6 m s^{-1}, (b) velocity 24 m s^{-1}.

The performance of the method for damage detection will be affected negatively by high levels of noise or road roughness. If the latter excited the modes of vibration of the vehicle sufficiently, the spectrum of the beam accelerations will contain vehicle frequencies in addition to the dominant bridge frequency. In this case, it may become necessary to apply a MAF to remove the 'dynamic' component associated to the vehicle motion in addition to the

MAF used for removing the natural frequency of the bridge. Provided that the frequency content of the 'damage' component is not altered to a large extent by noise, bridge, road or vehicle frequencies, the method will be able to detect damage. The lack of success in some scenarios will be related mainly to two factors: the portions at the ends of the response corrupted by axles entering and leaving the bridge, and the difficulty in safely removing frequencies interfering with the 'true' frequencies that define the 'damage' component.

6. Conclusions

The primary purpose of this paper has been to show how a localised loss in stiffness in a bridge beam model affects its acceleration response when it is traversed by a moving force and how his information can be exploited to detect damage. Many of the available signal processing techniques for damage detection demonstrate their effectiveness by analysing healthy and damaged signals and showing that a singularity that was not present in the healthy structure, appears in the response of the damaged structure. To the authors' knowledge, this paper is the first investigation that establishes the nature of the damage singularity in an acceleration response and discusses how the singularity changes with damage location and severity and with the properties of the beam and moving force. Understanding how this singularity manifests in the response is a crucial first step to improve the sensitivity of an algorithm to damage.

For this purpose, the total acceleration response has been divided into three distinctive components: 'dynamic', 'static' and 'damage'. A damage detection algorithm should aim to enhance the 'damage' component while hindering the influence of the other two components.

A number of issues have arisen when trying to highlight the 'damage' component. Firstly, the upper limit of the frequency range defining the singularity increases as the velocity of the force increases. Secondly, it has been shown that the location of the damage relative to the measuring location has a significant impact on the amplitude of the 'damage' component. The latter has important implications for operators trying to interpret the severity of damage. It has also been demonstrated that the ratio of the area under the 'damage' component to the area under the 'static' component is common across a range of bridge spans and force velocities. These ratios can then be used to quantify damage. Using a MAF to remove unwanted frequencies has been found to be effective because it preserves the area under the 'damage' and 'static' components (and obviously their ratios) while removing the 'dynamic' component. It has been shown that if the frequency range of the singularity contains bridge and/or vehicle frequencies, the 'damage' component cannot be isolated easily. The addition of a second moving force further increases the complexity of the problem due to the dependence of the results on the vehicle properties and the interference of forces entering and leaving the bridge. One way of addressing the challenge of a multi-axle vehicle is to derive the response due to a single point force from the total response due to a vehicle of known axle weights and spacings. The latter facilitates a common framework for identifying damage regardless of the vehicle configuration.

Acknowledgements

The authors wish to express their gratitude for the support received from the 7th European Framework Project ASSET (Advanced Safety and Driver Support for Essential Road Transport, 2008-2011) towards this investigation.

References

[1] C.R. Farrar, K. Worden, An introduction to structural health monitoring. Philosophical Transactions of the Royal Society 365 (2007) 303-315. doi:10.1098/rsta.2006.1928

[2] S. Doebling, C.R. Farrar, M.B. Prime, D.W. Shevitz, Damage identification and health monitoring of structural and mechanical systems from changes in their vibration characteristics: a literature review, Los Alamos National Laboratory report, LA-13070-MS, 1996.

[3] H. Sohn, C.R. Farrar, F.M. Hemez, D.D. Shunk, D.W. Stienmates, B.R. Nadler, A review of structural health monitoring literature: 1996-2001. Los Alamos National Laboratory report, LA-13976-MS, 2004.

[4] E.P. Carden, P. Fanning, Vibration based condition monitoring: a review. Structural Health Monitoring 3 (2004) 355-377. doi:10.1177/1475921704047500

[5] W. Fan, Q. Pizhong, Vibration-based damage identification methods: a review and comparative study. Structural Health Monitoring 10 (2010) 83-111. doi:10.1177/1475921710365419

[6] A. Messina, E.J. Williams, T. Contursi, Structural damage detection by a sensitivity and statistical-based method. Journal of sound and vibration 216 (1998) 791-808.

[7] B.P. Nandwana, S.K. Maiti, Detection of the location and size of a crack in stepped cantilever beams based on measurements of natural frequencies. Journal of Sound and Vibration 203 (1997) 435-446. doi:10.1006/jsvi.1996.0856

[8] O.S. Salawu, Detection of structural damage through changes in frequency: a review. Engineering Structures 19 (1997) 718-723. doi:10.1016/S0141-0296(96)00149-6

[9] J.J. Lee, J.W. Lee, J.H. Yi, C.B. Yun, H.Y. Jung, Neural networks-based damage detection for bridges considering errors in baseline finite element models. Journal of Sound and Vibration 280 (2005) 555-578. doi:10.1016/j.jsv.2004.01.003

[10] C. Hu, M.T. Afzal, A statistical algorithm for comparing mode shapes of vibration testing before and after damage in timbers. Journal of Wood Science 52 (2006) 348-352. doi: 10.1007/s10086-005-0769-9

[11] V. Pakrashi, A. O'Connor, B. Basu, A study on the effects of damage models and wavelet bases for damage identification and calibration in beams. Computer-Aided Civil and Infrastructure Engineering 22 (2007) 555-569. doi:10.1111/j.1467-8667.2007.00510.x

[12] A. Gentile, A. Messina, On the continuous wavelet transforms applied to discrete vibrational data for detecting open cracks in damaged beams. International Journal of Solids and Structures 40 (2003) 259-315.

[13] S. Douka, S. Loutridis, A. Trochidis, Crack identification in beams using wavelet analysis. International Journal of Solids and Structures 40 (2003) 3557-3569. doi:10.1016/S0020-7683(03)00147-1

[14] A.C. Okafor, A. Dutta, Structural damage detection in beams by wavelet transforms. Smart Materials and Structures 9 (2000) 906-917.

[15] O. Huth, G. Feltrin, J. Maeck, N. Kilic, M. Motavalli, Damage identification using modal data: experiences on a prestressed concrete bridge. Journal of Structural Engineering 131 (2005) 1898-1910.

[16] A.K. Pandey, M. Biswas, M.M. Samman, Damage detection from changes in curvature mode shapes. Journal of Sound and Vibration 145 (1991) 321-332. doi:10.1016/0022-460X(91)90595-B

[17] C.P. Ratcliffe, Damage detection using a modified Laplacian operator on mode shape data. Journal of Sound and Vibration 204 (1997) 505-517. doi:10.1006/jsvi.1997.0961

[18] B.H. Kim, T. Park, G.Z. Voyiadjis, Damage estimation on beam-like structures using the multi-resolution analysis. International Journal of Solids and Structures 43 (2006) 4238-4257. doi:10.1016/j.ijsolstr.2005.07.022

[19] K.J. Sinha, M.I. Friswell, S. Edwards, Simplified models for the location of cracks in beam structures using measured vibration data. Journal of Sound and Vibration 251 (2002) 13-38. doi:10.1006/jsvi.2001.3978

[20] A. Teughels, G. De Roeck, Structural damage identification of the highway bridge Z24 by FE model updating. Journal of Sound and Vibration 278 (2004) 589-610.

[21] X.Q. Zhu, S.S. Law, Wavelet-based crack identification of bridge beam from operational deflection time history. International Journal of Solids and Structures 43 (2006) 2299-2317. doi:10.1016/j.ijsolstr.2005.07.024

[22] W. Zhang, Z. Wang, H. Ma, Studies on wavelet packet-based crack detection for a beam under the moving load. Key Engineering Materials 413 (2009) 285-290. doi:10.4028/www.scientific.net/KEM.413-414.285

[23] D. Hester, A. González, A wavelet-based damage detection algorithm based on bridge acceleration response to a vehicle. Mechanical Systems and Signal Processing, in press, available online July 2011. doi:10.1016/j.ymssp.2011.06.007

[24] M. Bradley, A. González, A., D. Hester, Analysis of the structural response to a moving load using empirical mode decomposition, in: Frangopol, Sause, Kusko (Eds.), Bridge Maintenance , Safety, Management and Life-cycle optimization. Taylor & Francis, London, 2010, pp. 356-363.

[25] N.E. Huang, K. Huang, W.-L. Chiang, HHT based bridge structural health monitoring method, in: Huang, N.E., Shen, S.S.P. (Eds.), Hilbert-Huang Transform and its Applications. World Scientific Publishing, Singapore, 2005, pp. 263-287.

[26] C.W. Rowley, Moving Force Identification of Axel Forces on Bridges. PhD Thesis, University College Dublin, Ireland, 2007

[27] Y.W. Kwon, H. Bang, The Finite Element Method Using Matlab, CRC Press, Inc., Boca Raton, FL, 237-244, 2000.

[28] J.W. Tedesco, W.G. McDougal, C.A. Ross, Structural Dynamics: Theory and Applications, Addison Wesley Longman Inc, Menlo Park CA, 1999.

[29] R.V. Dukkipati, MATLAB for Mechanical Engineers, New Age Science, 2009.

[30] A.D. Dimarogonas, Vibration of cracked structures: a state of the art review. Engineering Fracture Mechanics 55 (1996) 831-857. doi:10.1016/0013-7944(94)00175-8

[31] M.A. Mahmoud, Effect of cracks on the dynamic response of a simple beam subject to a moving load. Proceedings of the Institute of Mechanical Engineers, Part F: Journal of Rail and Transit 15 (2001) 207-215. doi:10.1243/0954409011531521

[32] D. Hester, A. González, C.W. Rowley, Examining the dynamic response of a deteriorated bridge due to the passage of moving loads, in Proceedings of the Bridge and Infrastructure Research Symposium in Ireland, Galway, Ireland, 2008, pp. 111-119.

[33] A. González, D. Hester, The use of wavelets on the response of a beam to a calibrated vehicle for damage detection, Proceedings of the 7th International Symposium on Non-destructive Testing in Civil Engineering, Nantes, France, June-July 2009, pp. 743-748.

[34] K.V. Nguyen, H.T. Tran, Multi-cracks detection of a beam like structure based on the on-vehicle vibration signal and wavelet analysis. Journal of Sound and Vibration 329 (2010) 4455-4465. doi:10.1016/j.jsv.2010.05.005

[35] Yang, Y.B., J.D. Yau, and Y.S. Wu, Vehicle-bridge interaction dynamics: with applications to high-speed railways, World Scientific Pub Co Inc, 2004

[36] A. González, Development of a bridge Weigh in Motion System, Lambert Academic Publishing, Saarbrucken Germany, 2010.

[37] E.J. OBrien, M.J. Quilligan, R. Karoumi, Calculating an influence line from direct measurements. Bridge Engineering, Proceedings of the Institution of Civil Engineers 159 (2006) 31-34. doi:10.1680/bren.2006.159.1.31

[38] M.F. Green, D. Cebon, Dynamic interaction between heavy vehicles and highway bridges. Computers and Structures 62 (1997) 253-264. doi:10.1016/S0045-7949(96)00198-8

[39] F. Yang, G.A. Fonder, An iterative solution method for dynamic response of bridge-vehicle systems. Earthquake Engineering and Structural Dynamics 25 (1996) 195-215. doi: 10.1002/(SICI)1096-9845(199602)25:2<195::AID-EQE547>3.0.CO;2-R

[40] M.M. El-Madany, Design optimization of truck suspension using covariance analysis. Computers and Structures 28 (1988) 241-246. doi:10.1016/0045-7949(88)90045-4

[41] N.K. Harris, E.J. OBrien, A. González, Reduction of bridge dynamic amplification through adjustment of vehicle suspension damping. Journal of Sound and Vibration 302 (2007) 471-485. doi:10.1016/j.jsv.2006.11.020

List of Figures

Fig. 9. Estimated ‘static’ (or filtered total) and ‘damage’ components for different damage scenarios in a 40 m bridge traversed by a force at 6 m s^{-1}.

Fig. 10. Ratios of ‘damage’ area to ‘static’ area with respect to the position of damage.

Fig. 11. Extraction of ‘damage’ component from filtered total acceleration.

Fig. 12. Location and quantification of damage based on the prediction of ratio ’damage’ to ‘static’ area obtained for different damage scenarios (’40m,0.2@0.33L, 6 m s^{-1}‘ in the figure indicates the bridge had a 40 m span with a damage of delta = 0.2 at 0.33L and was traversed by a force at 6 m s^{-1}).

Fig. 13. Detecting multiple damages (a) Extraction of ‘damage’ component from filtered mid-span acceleration with two damaged locations; (b) location and quantification of damage based on ratio of ‘damage’ to ‘static’ area for two different levels of damping.

Fig. 14. Mid-span acceleration response due to two constant forces crossing a 40 m bridge: (a) total acceleration response; (b) ’ dynamic’ component of acceleration; (c) ‘static’ and ‘damage’ components of acceleration; (d) filtered total acceleration.

Fig. 15. Location and quantification of damage based on prediction of ratio ’damage’ to ‘static’ area obtained from mid-span accelerations due to two-constant forces for different damage scenarios. Span (m): O 40, □ 20 and Δ 10; damage severity: delta = 0.2 (large marker size) and delta = 0.1 (small marker size). (a) velocity 6 m s^{-1}, (b) velocity 24 m s^{-1}.

.

Fig. 16. Location and quantification of damage based on ratio 'damage' to 'static' area obtained from mid-span accelerations due to a two-axle sprung vehicle model on a smooth profile for different damage scenarios. Span (m): O 40, □ 20 and Δ 10; damage severity: delta = 0.2 (large marker size) and delta = 0.1 (small marker size). (a) velocity 6 m s^{-1}, (b) velocity 24 m s^{-1}.

List of Tables

Table 1. Parameters of bridge models.

Table 2. Parameters of vehicle model.

Figure 1

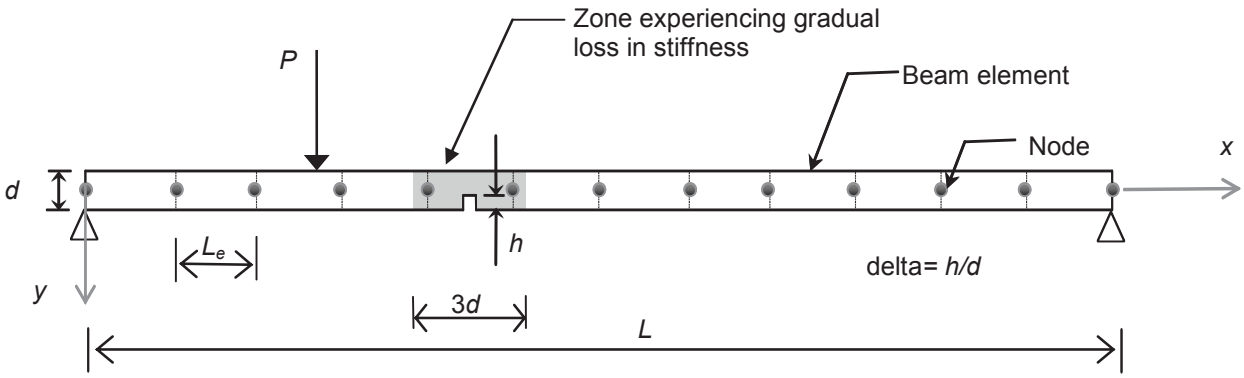
Zone experiencing gradual
loss in stiffness
P
Beam element
Node
x
d
L_e
h
y
delta= h/d
3d
L

Figure 2
Click here to download high resolution image

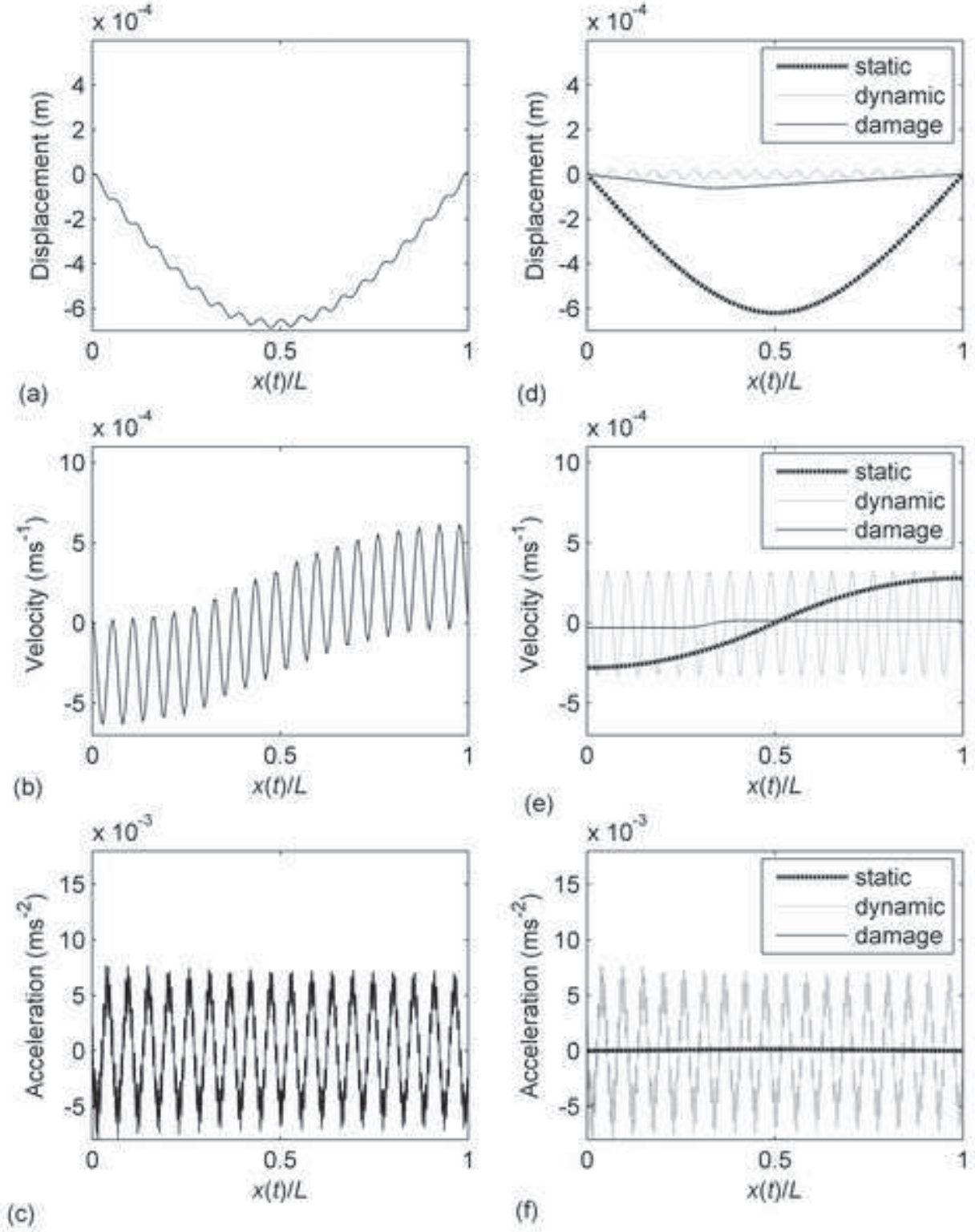

figure3

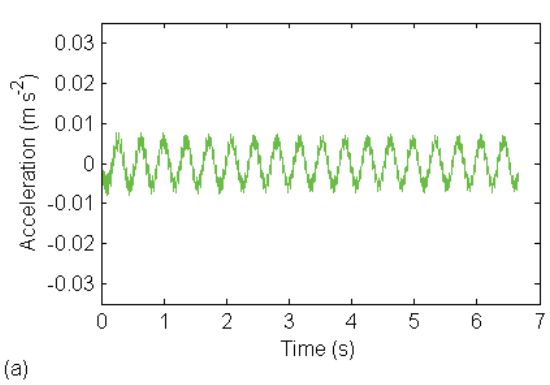

(a)

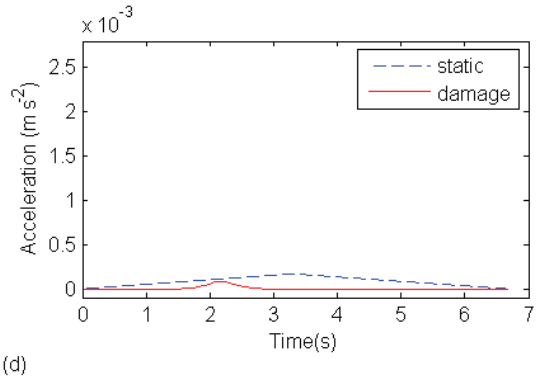

(d)

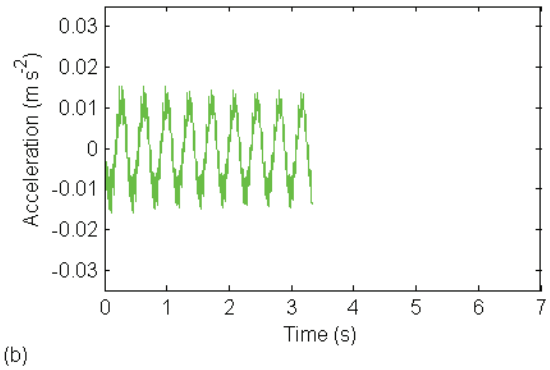

(b)

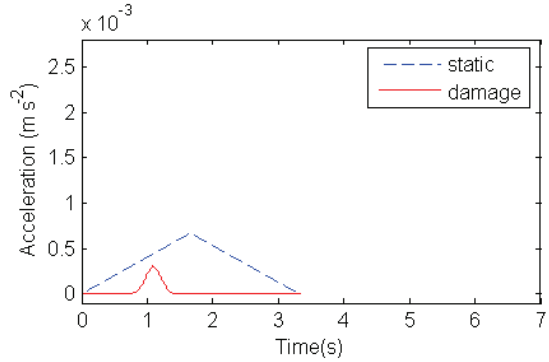

(e)

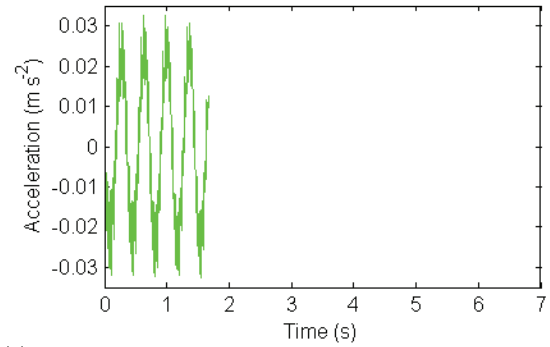

(c)

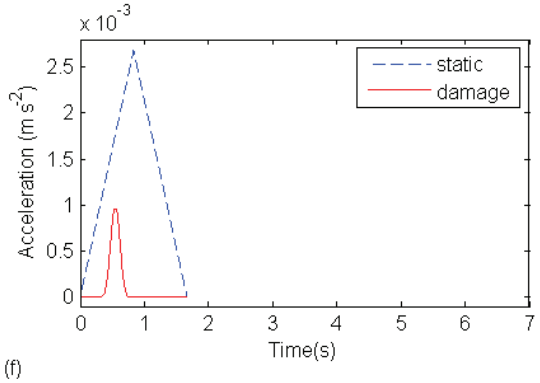

(f)

figure4

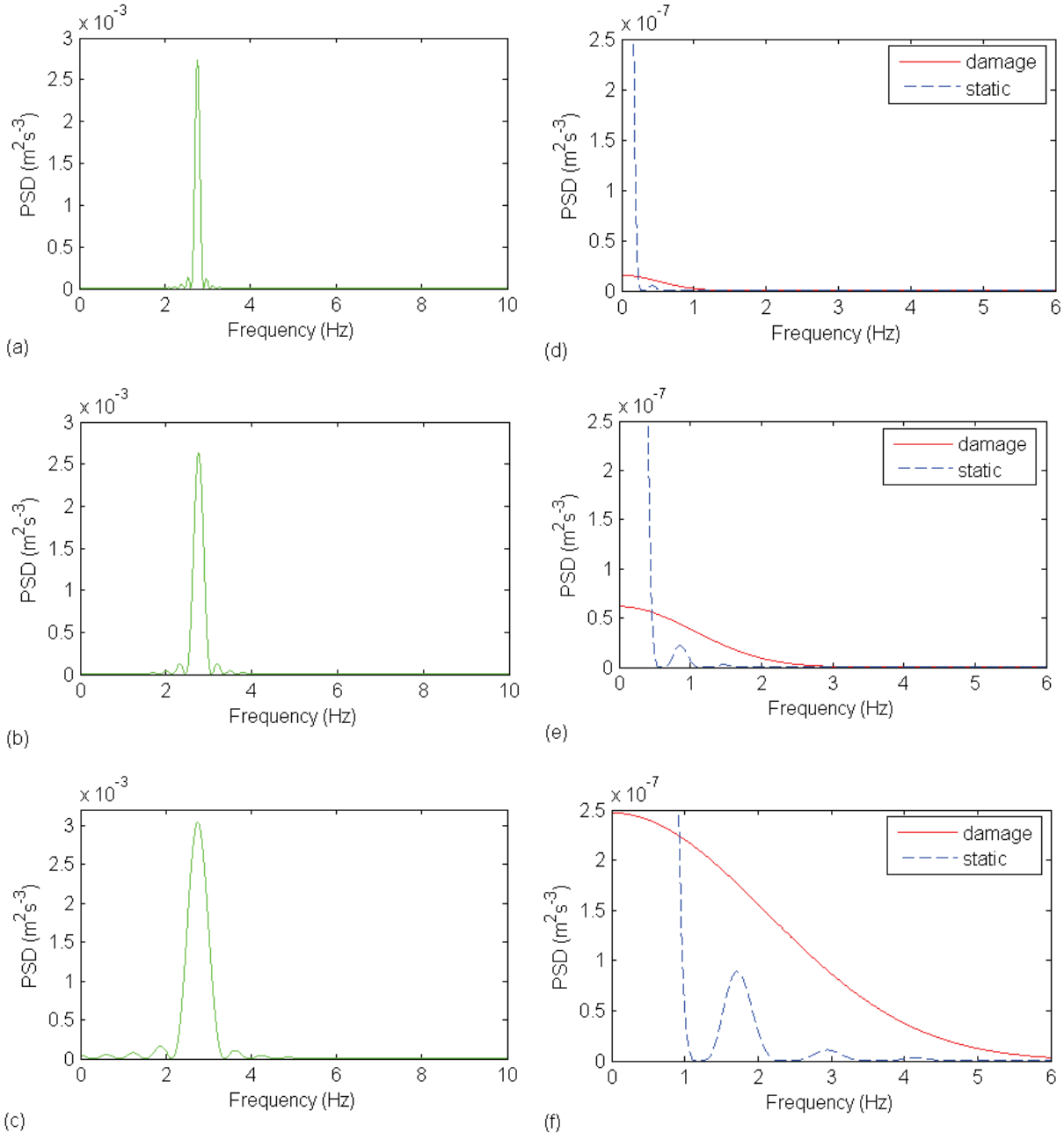

Figure 5
Click here to download high resolution image

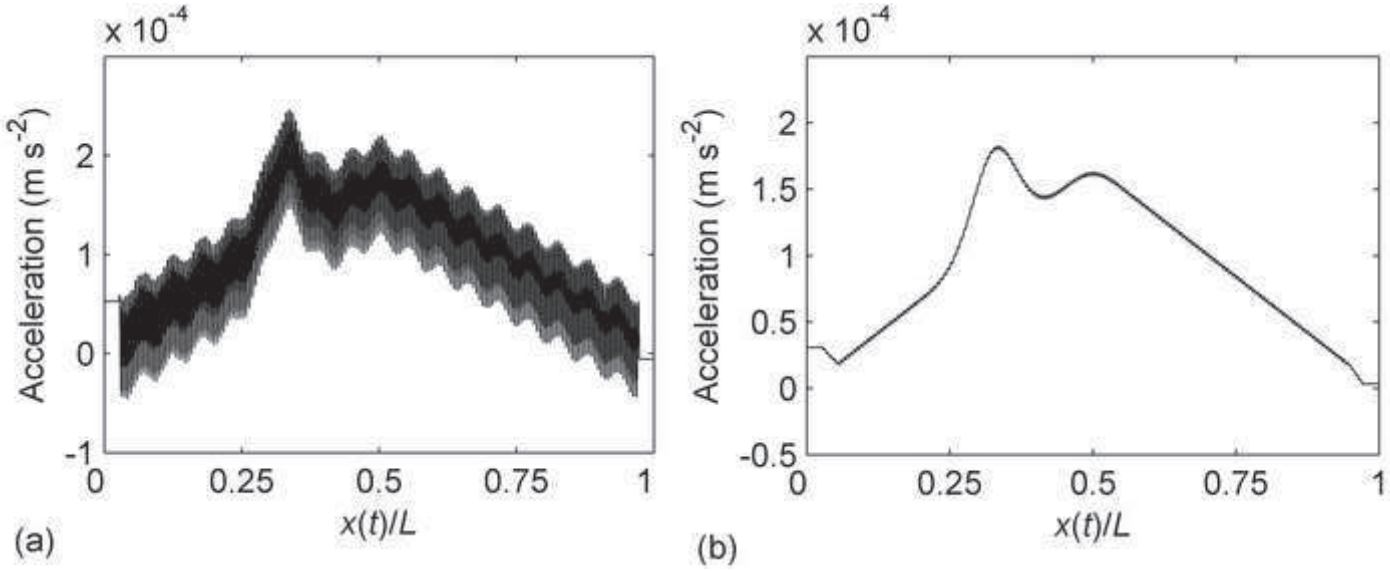

Figure 6
Click here to download high resolution image

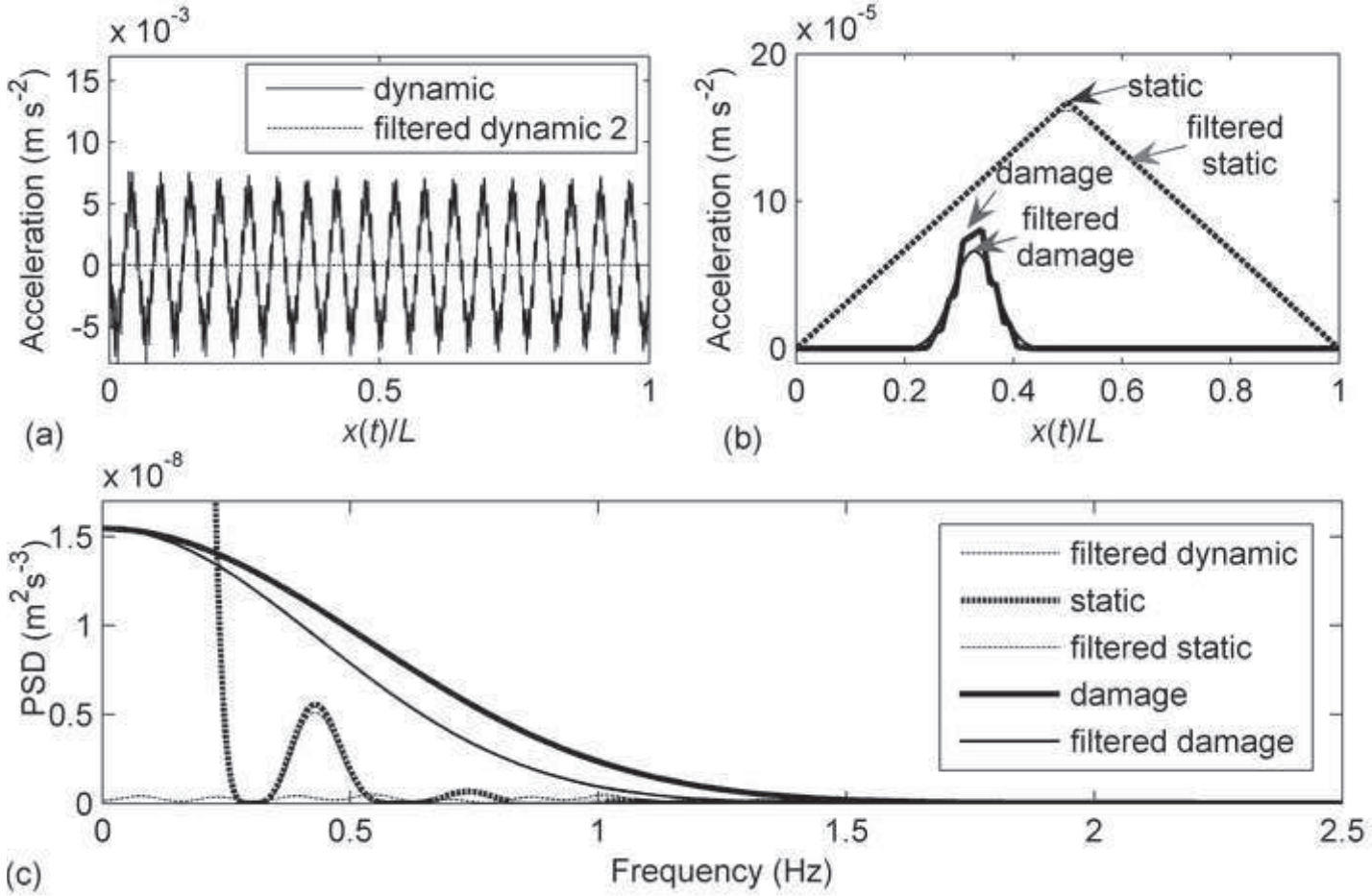

Figure 7
Click here to download high resolution image

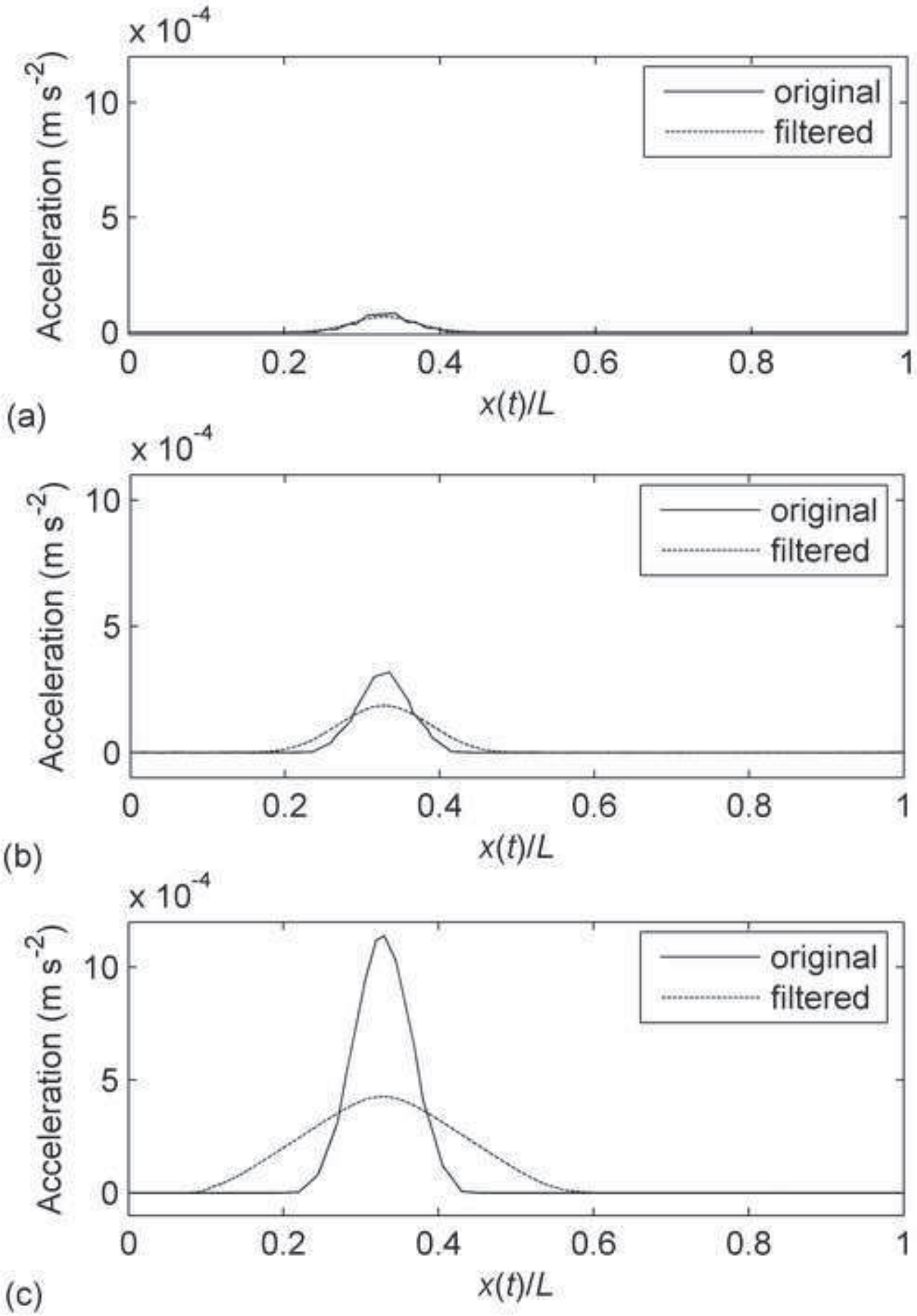

Figure 8
Click here to download high resolution image

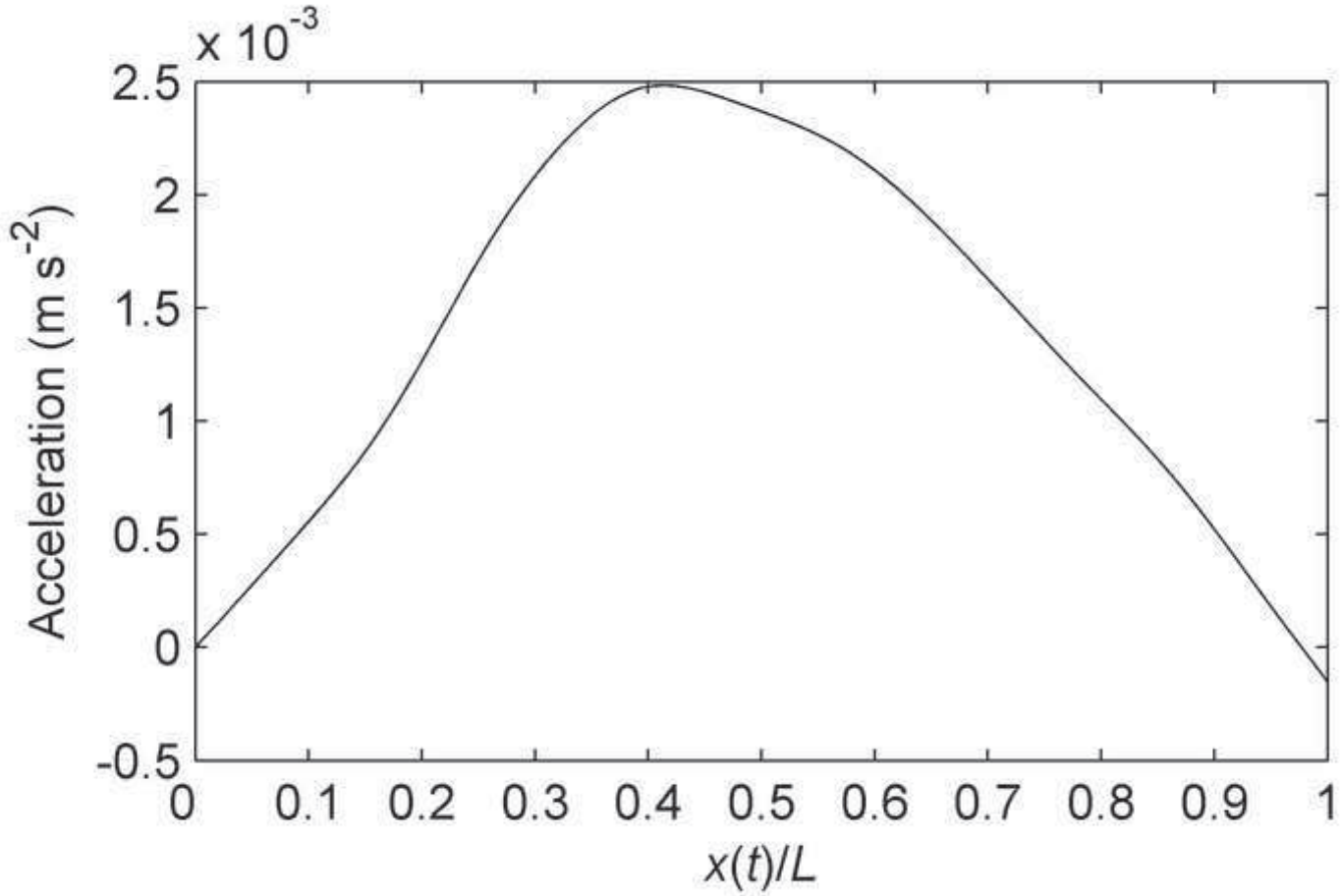

Figure 9
Click here to download high resolution image

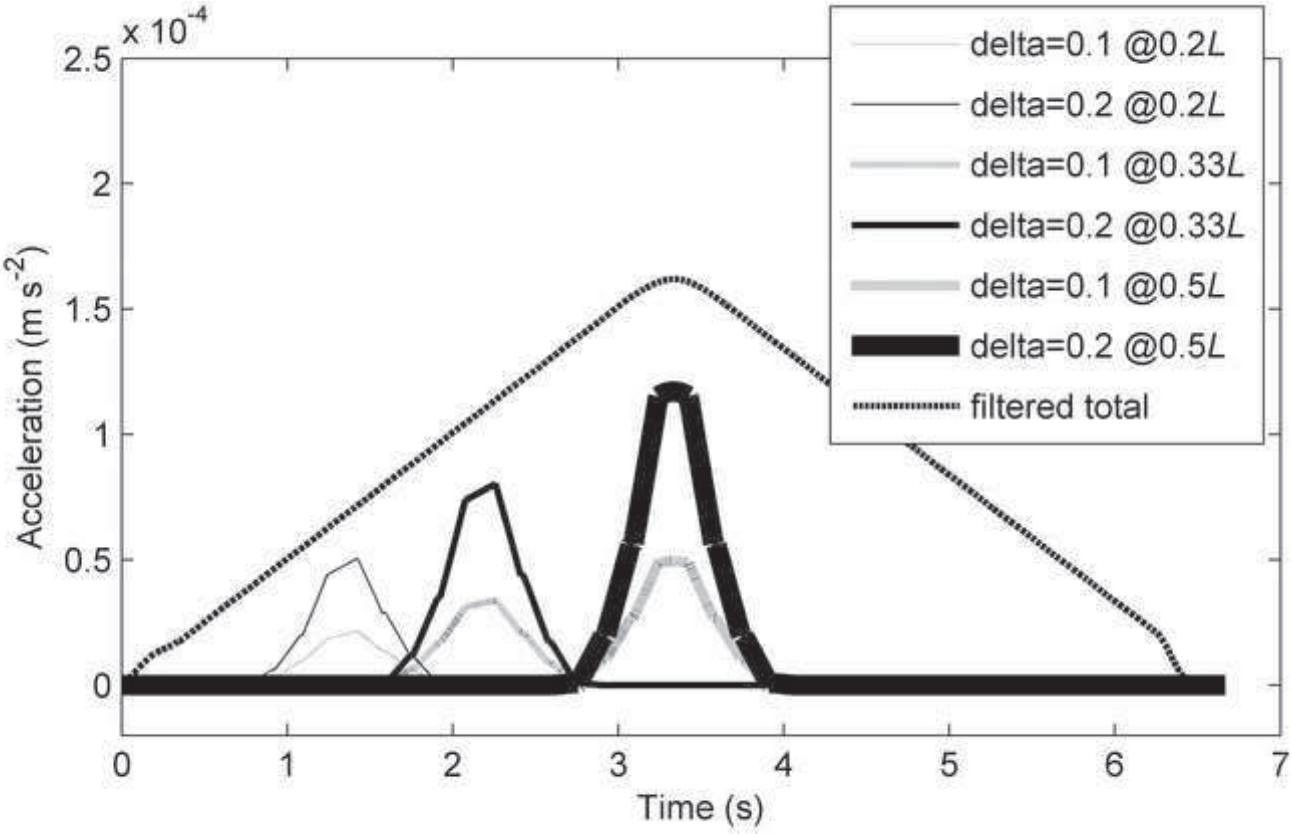

figure10
Click here to download high resolution image

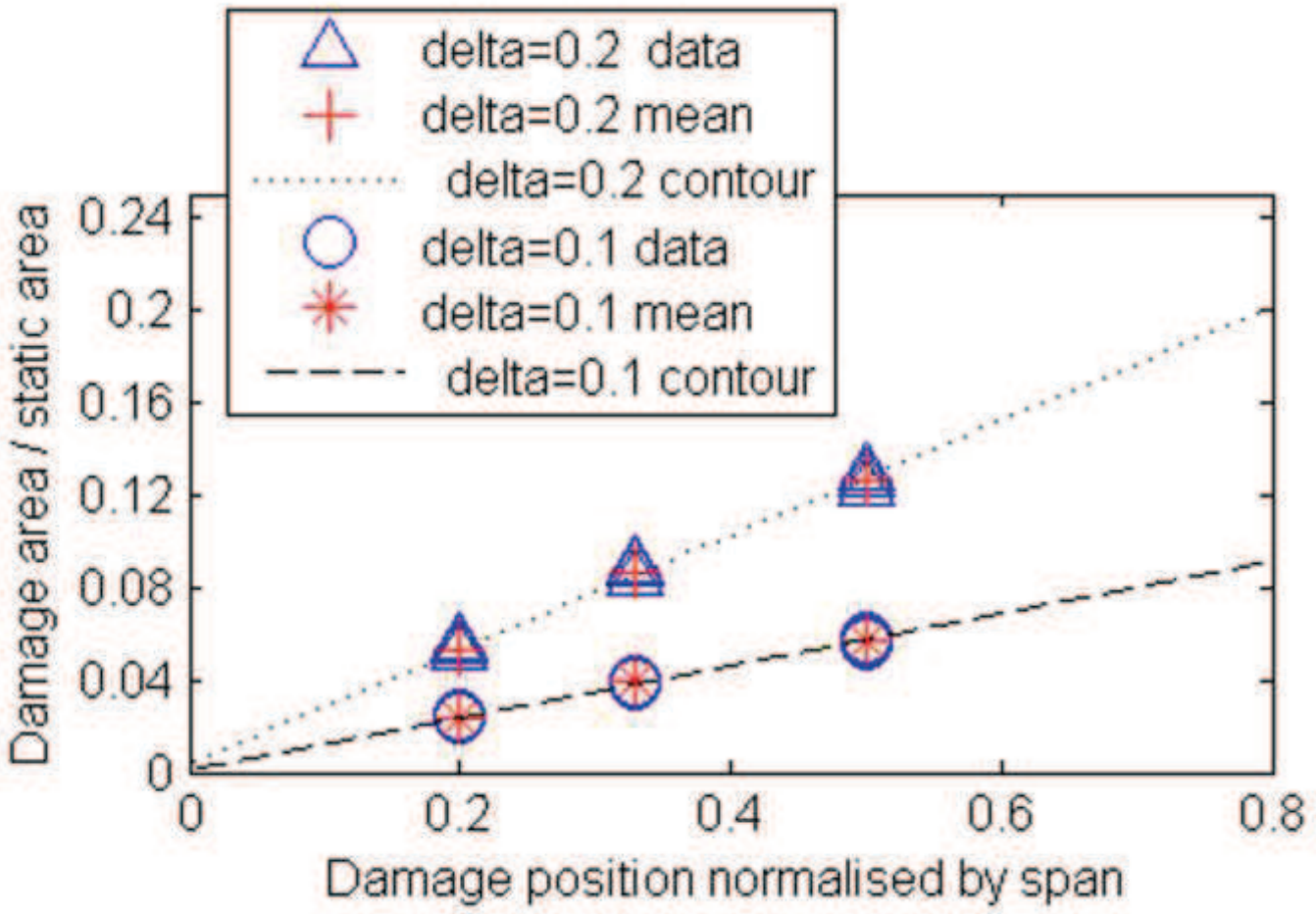

Figure 11
Click here to download high resolution image

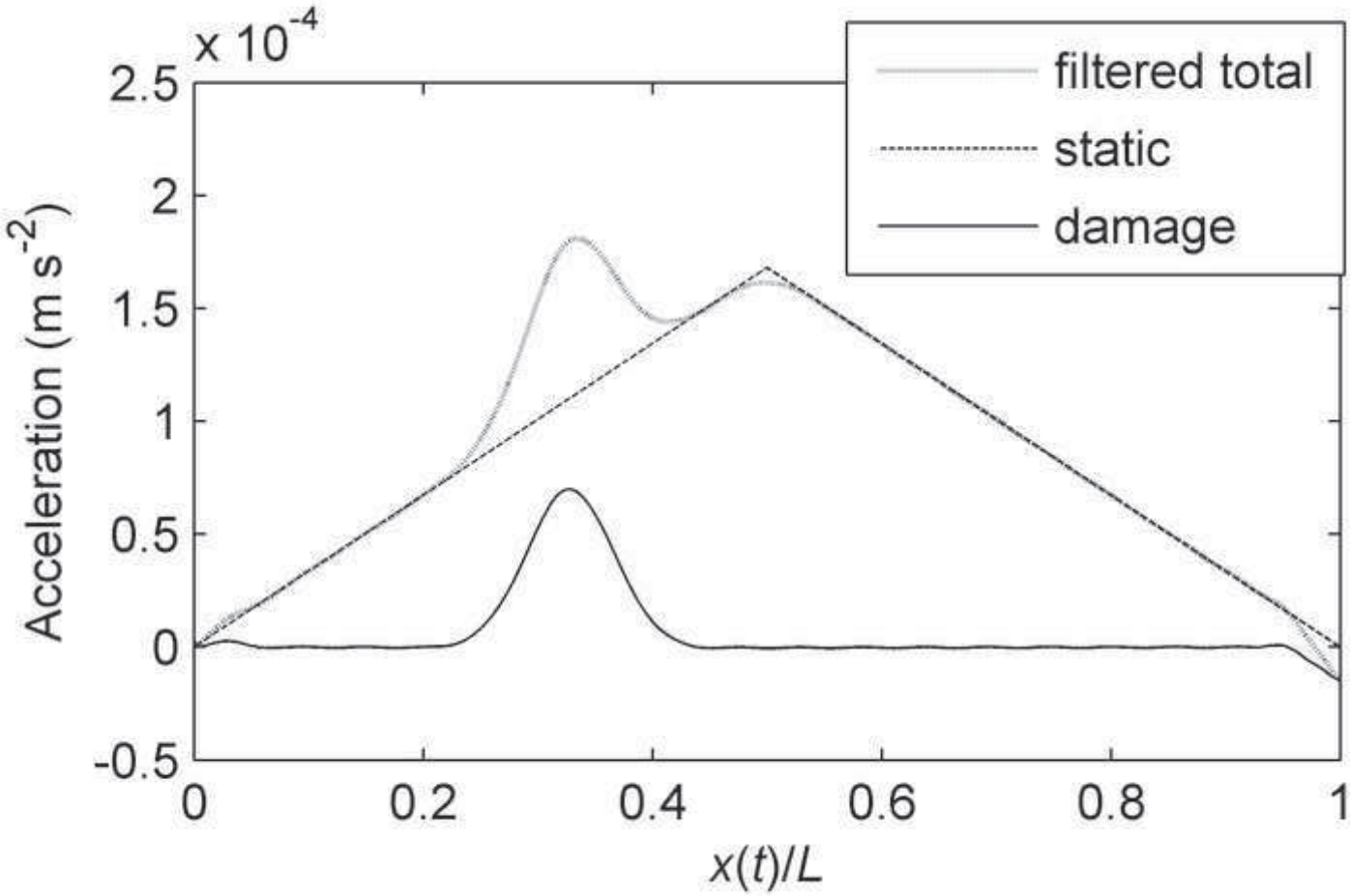

Figure 12
Click here to download high resolution image

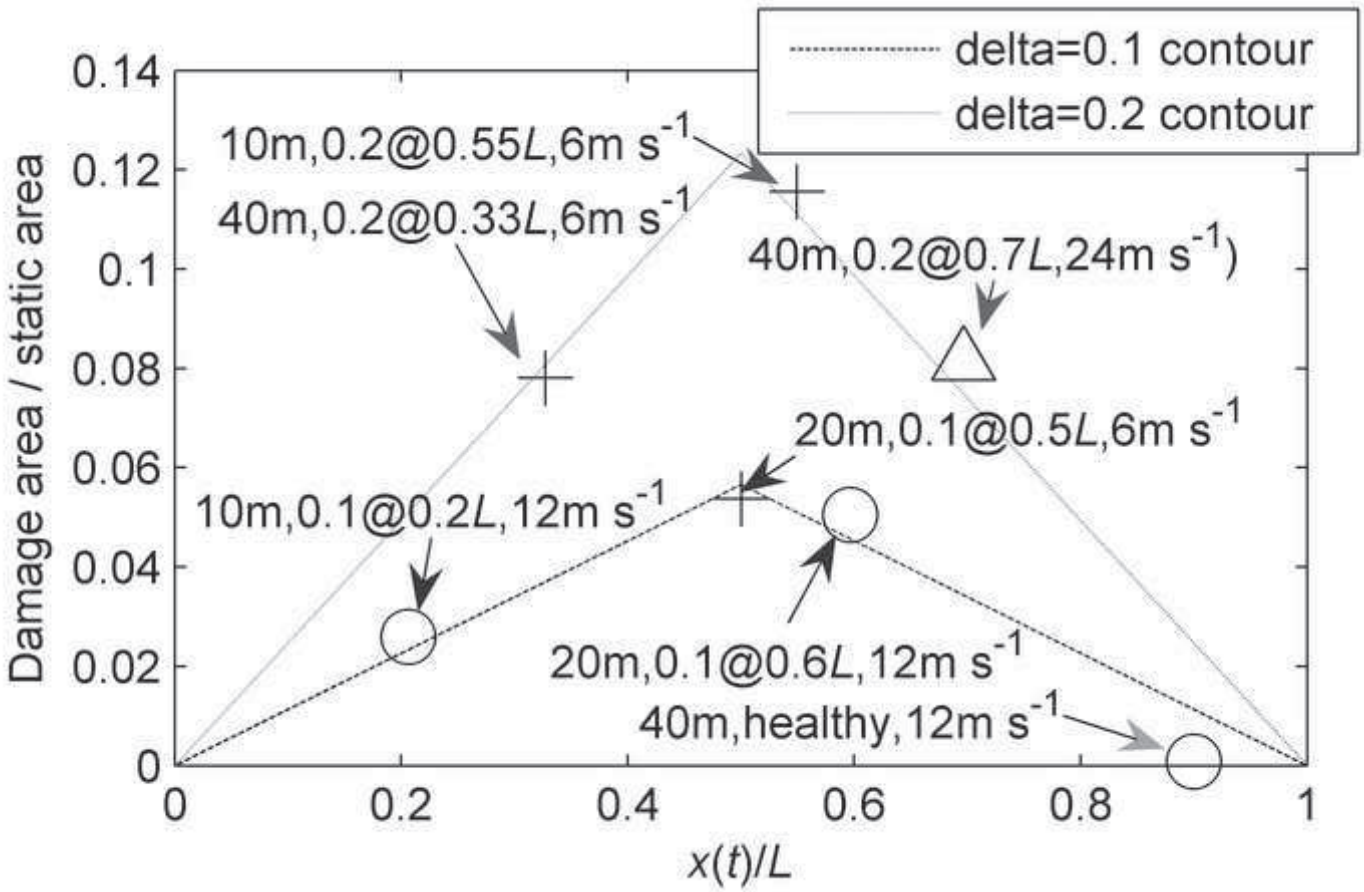

Figure 13
Click here to download high resolution image

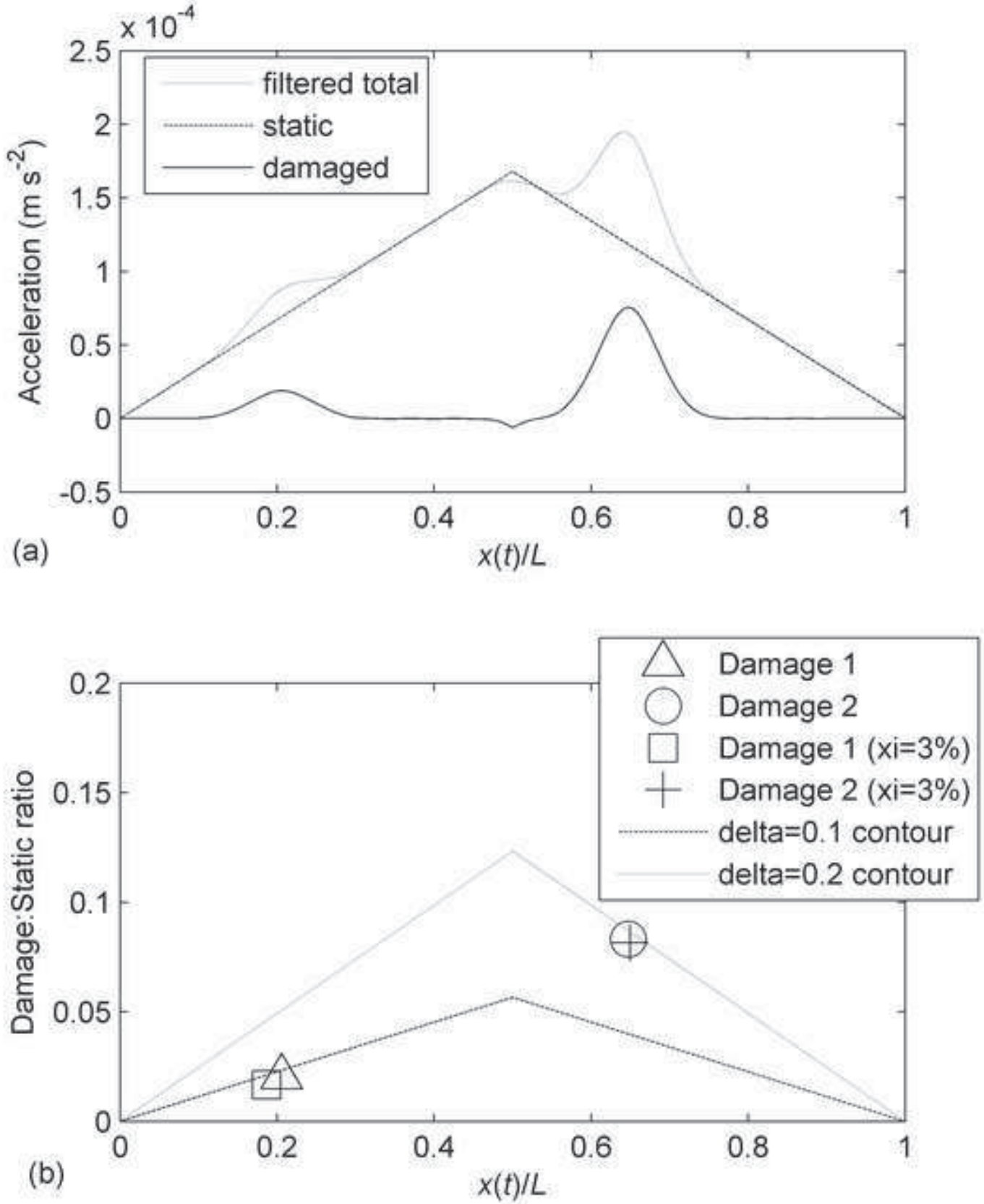

figure14
Click here to download high resolution image

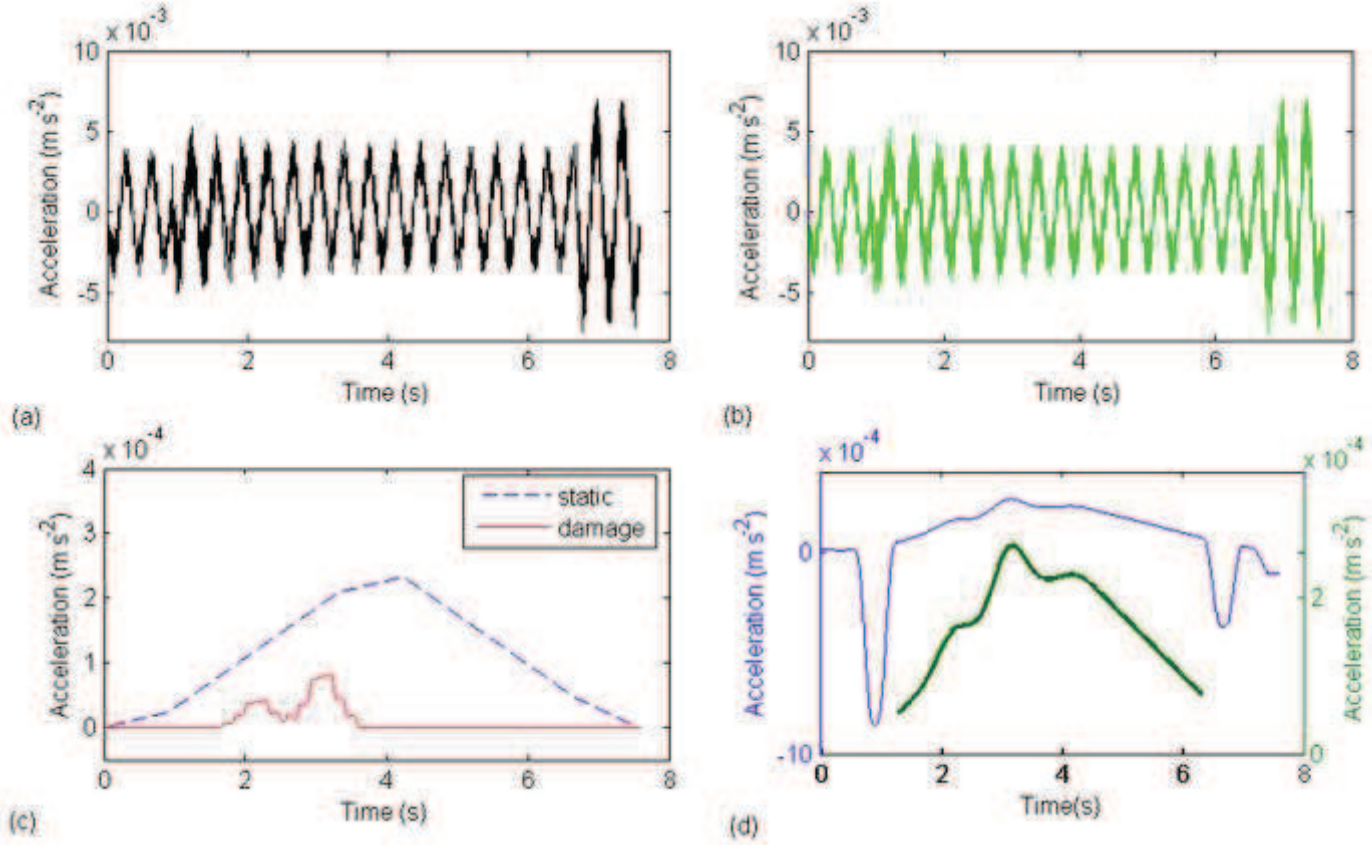

Figure 15a
Click here to download high resolution image

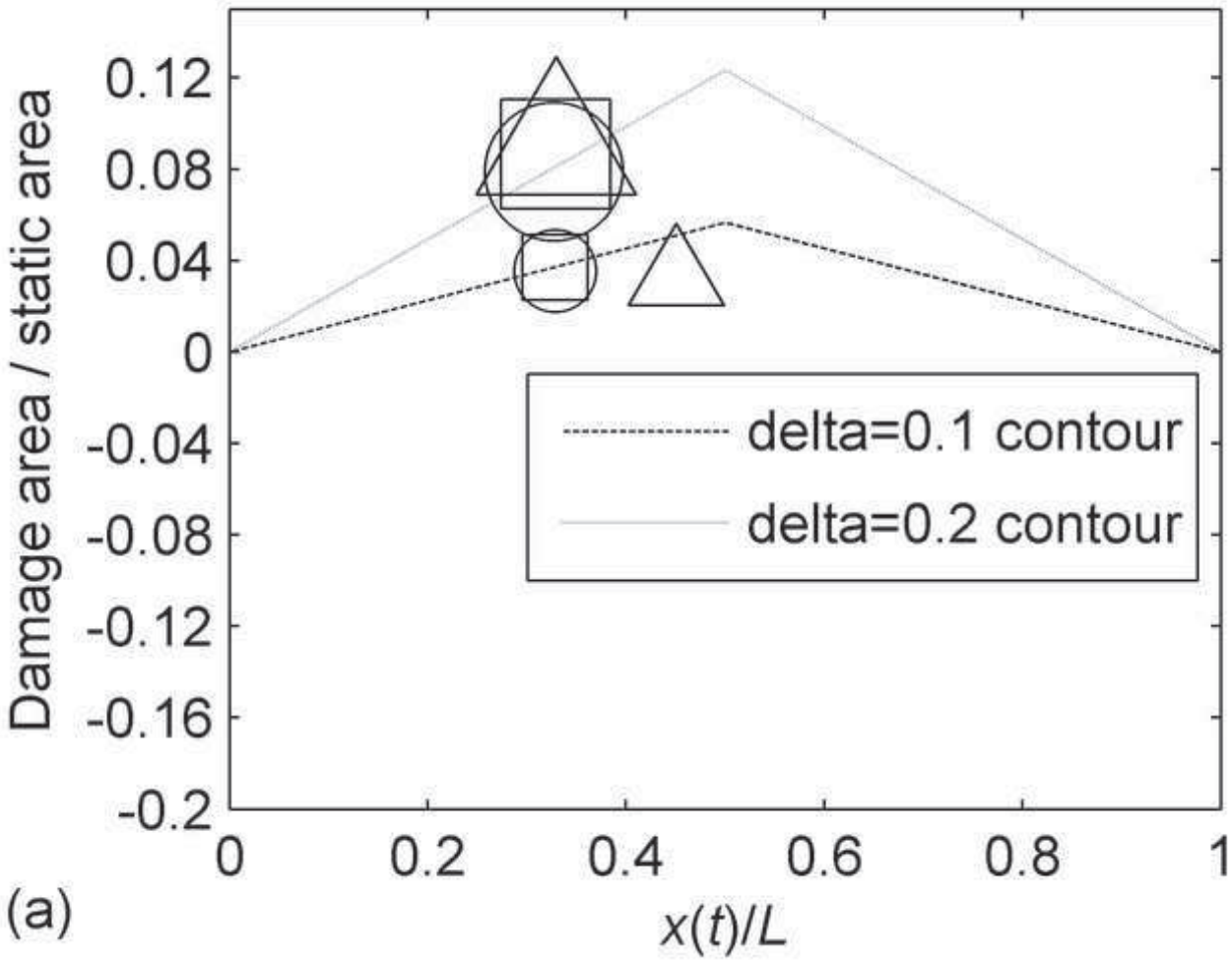

Figure 15b
Click here to download high resolution image

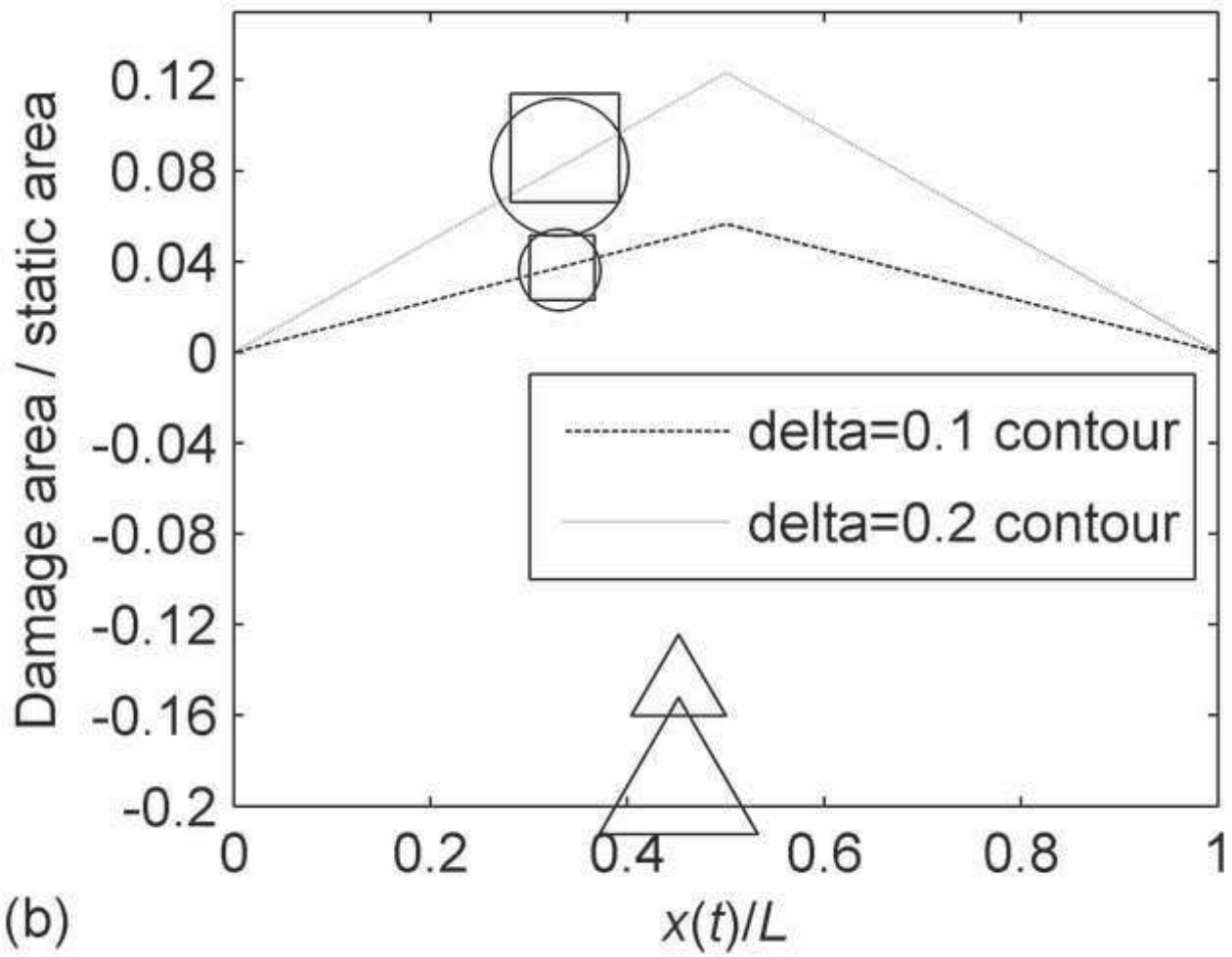

Figure 16a
Click here to download high resolution image

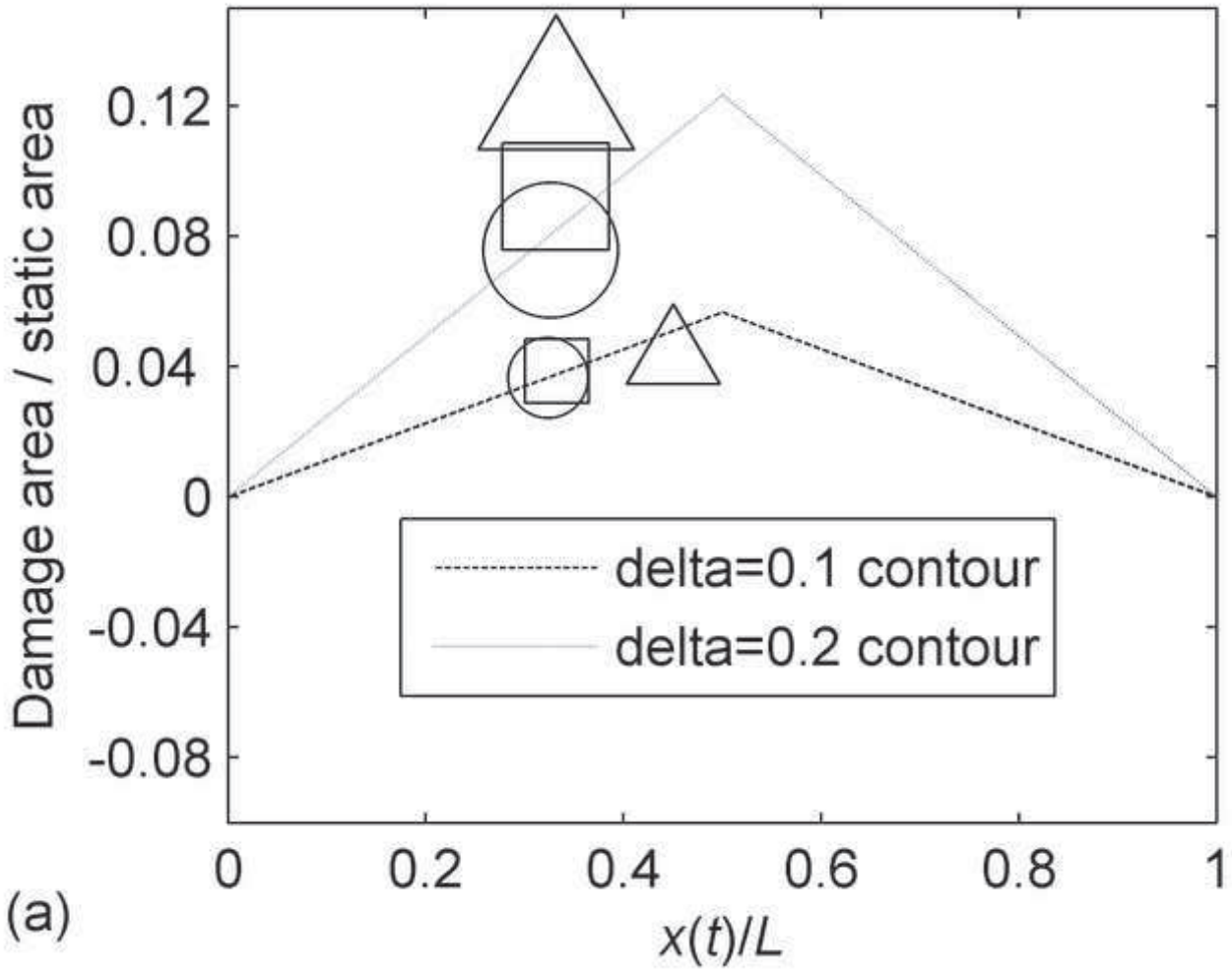

Figure 16b
Click here to download high resolution image

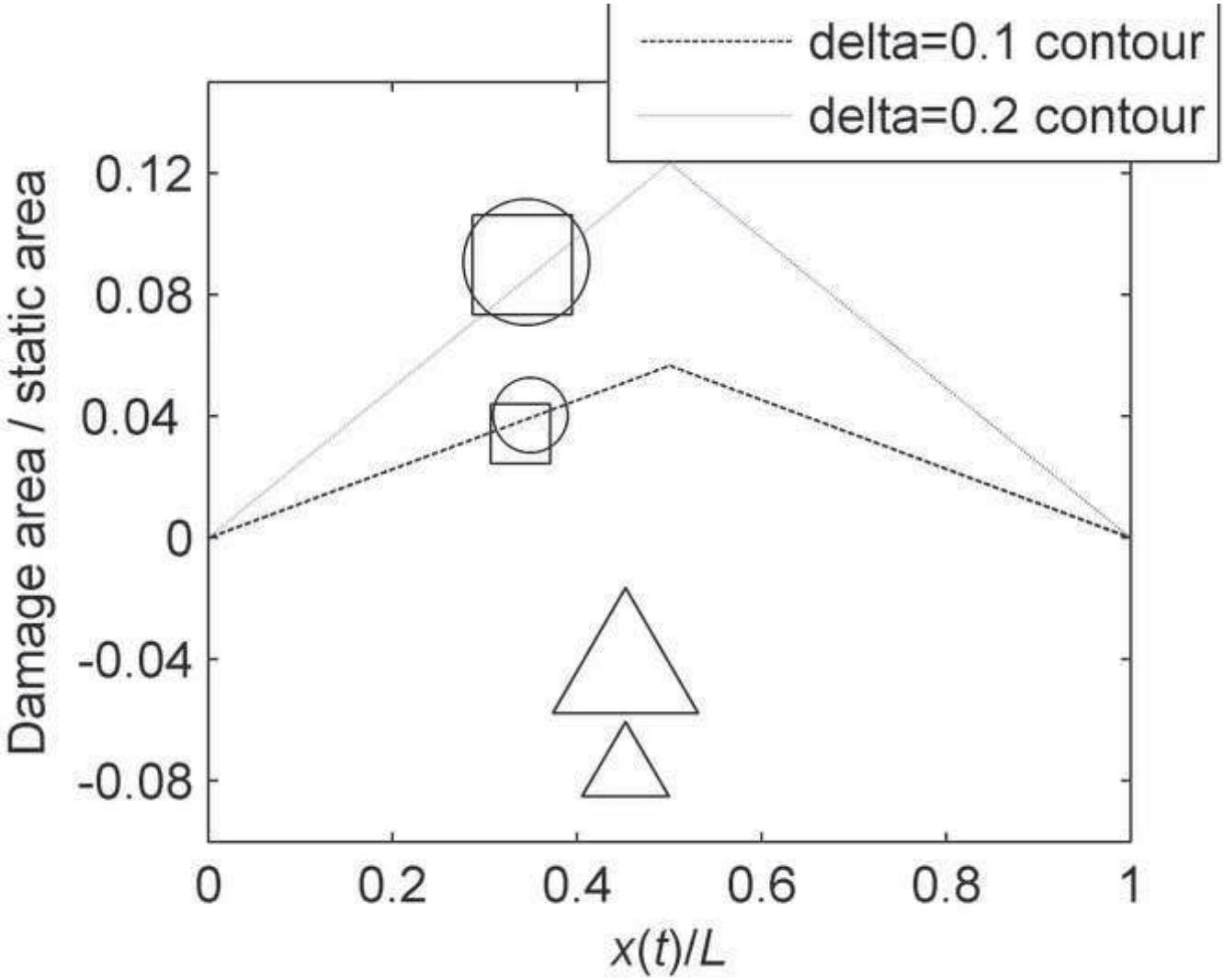

table1

span (m)	width (m)	inertia (m^4)	modulus of elasticity (N m^{-2})	area (m^2)	1st natural frequency (Hz)
40	15	6.00	$3.5x10^{10}$	10.0	2.88
20	15	1.36	$3.5x10^{10}$	7.3	6.24
10	15	0.28	$3.5x10^{10}$	9.1	10.40

table2

dimensional data (m)		
	wheel base	5.5
	dist from centre of mass to front axle	3.63
	dist from centre of mass to rear axle	1.87
	overall length of truck	6.5
mass and inertia		
mass (kg)	front axle mass	700
	rear axle mass	1,100
	sprung body mass	13,300
inertia (kg m^2)	pitch moment of inertia of truck	41,008
suspension		
spring stiffness (kN m^{-1})	front axle	400
	rear axle	1,000
damping (kN s m^{-1})	front axle	10
	rear axle	10
tyre stiffness (kN m^{-1})	front axle	1,750
	rear axle	3,500